Human macula formation involves two waves of retinoic acid suppression via *CYP26A1* that modulate cell cycle exit and cone subtype specification

Philippa Harding[1*], Maja Wojtynska[1], Alexander J. Smith[1], Robin R. Ali[1], Rachael A. Pearson[1†**]

[1]Ocular Cell and Gene Therapy Group, Centre for Gene Therapy and Regenerative Medicine, King's College London, Tower Wing, Guy's Hospital, London, SE1 9RT, UK

[*]Corresponding authors: *philippa.harding@kcl.ac.uk; **rachael.pearson@kcl.ac.uk

†Lead contact

Summary

The human macula is a specialized, cone-rich region of the eye, critical for high-acuity vision, yet the pathways regulating its development remain poorly understood. RA-catabolizing enzyme *CYP26A1* establishes the chick high-acuity area via upregulation of *FGF8*. However, detailed analysis of this pathway and its functions has not been performed in early human fetal tissue. Fluorescent *in situ* hybridization revealed striking biphasic *CYP26A1* expression but little *FGF8* in the presumptive macula region between post-conception weeks (PCW)6-17. Pharmacological RA signaling inhibition in human retinal organoids mimicking the two waves of *CYP26A1* revealed early RA inhibition prompted early cell cycle exit and increased cone genesis, while late inhibition altered cone subtype specification. Conversely, recombinant FGF8 had no effect on photoreceptor fate. This work provides spatiotemporal examination of *CYP26A1* across human macular development, as well as experimental evidence for the different roles of RA signaling inhibition in a human model of retinal development.

Introduction

The macula is a 5-6mm region at the center of the retina, containing within it the fovea, an area critical for high-acuity and color vision in humans and simian primates(Hoshino *et al.*, 2017; Voigt *et al.*, 2021). Damage and degeneration in this region lead to debilitating sight loss, significantly impacting activities such as reading and recognizing faces. The macula has a unique architecture comprising a high density of cone photoreceptors, contrasting with the rod-dominant peripheral retina, the highest density (200,000 cones/mm^2) being at the center of the macula in the foveola, a 300μm avascular rod-free zone (RFZ) consisting exclusively of medium (M/green) and long (L/red) wavelength-detecting cones(Curcio *et al.*, 1990; Voigt *et al.*, 2021). The proportion of cones:rods declines with increasing eccentricity, being ~1:1 in the fovea, dropping to 1:30 in the peripheral retina. Additionally, the macula contains the highest density of retinal ganglion cells (RGCs) in the retina, and a highly ordered synaptic configuration to aid rapid phototransduction.

The retina exhibits a striking center-to-periphery gradient of development, the central retina entering neurogenesis ~50 days before peripheral regions(Hoshino *et al.*, 2017), whilst macular differentiation precedes even the equivalent region in the nasal retina, with immature cones present in the presumptive macula (PM) by the end of post-conception week (PCW)8/Carnegie stage (CS)23(Hendrickson and Zhang, 2019). However, due to central migration of cones into the fovea, adult cone density is not achieved until 4-6 years(Curcio *et al.*, 1990). Despite their importance, the molecular mechanisms underlying human macular and foveal development remain poorly understood, owing to the lack of equivalent structures in classical animal models. Furthermore, minimal evaluation of macular formation has been performed in human tissue prior to PCW8, due to limited tissue samples, and the lack of a macular marker expressed at this early stage(Hendrickson,

46 2016). Some other species do possess a broadly analogous high-acuity region; Chickens possess an
47 RFZ, called the *area centralis* or High-Acuity Area (HAA)(Mey and Thanos, 2000). Recent research has
48 shown that chick HAA formation is dependent on regulation of retinoic acid (RA) levels(Silva and Cepko,
49 2017). RA is a morphogen that can control gene expression through binding to RA receptors (RARs)
50 and retinoid X receptors (RXRs), which then engage RA-response elements (RAREs)(Cvekl and Wang,
51 2009). Upon binding to RAREs, co-activators are recruited and lead to transcriptional regulation of
52 specific RA-regulated genes(Cunningham and Duester, 2015). RA is synthesized by retinal
53 dehydrogenases (ALDHA1-3) and catabolized by cytochrome P450 family 26 enzymes (CYP26s) (Cvekl
54 and Wang, 2009).
55
56 In the developing chick retina, strong expression of *Cyp26a1/c1* was observed at a single spot at the
57 presumptive HAA early, coincident and colocalized with similarly strong expression of *Fgf8* (fibroblast
58 growth factor 8), which is otherwise downregulated by RA(Cunningham and Duester, 2015; Silva and
59 Cepko, 2017). Accordingly, transient addition of RA led to loss of *Fgf8* expression, and disruption of the
60 RFZ and a decrease in the high RGC density typical of the HAA(Silva and Cepko, 2017). In the same
61 study, expression of *CYP26A1* mRNA was observed in the human PM at CS22 (late PCW8), indicating a
62 potentially conserved signaling pathway in HAA/macula development. In support of this, increased
63 expression of *Cyp26a1* by Müller glia (MG) has been observed, albeit much later in development, in
64 the zebrafish HAA(Lahne, Yoshimatsu and MacDonald, 2023), macaque and marmoset(Peng *et al.*,
65 2019; Krueger *et al.*, 2024), and bulk and scRNAseq studies have reported *CYP26A1* to be significantly
66 upregulated in human macula compared with peripheral retina in mid-gestation (PCW20) and in the
67 MG of adult retina human retina(Peng *et al.*, 2019; Cowan *et al.*, 2020). Notably, recent detailed
68 analysis of *CYP26A1* and *FGF8* expression in macaque(Krueger *et al.*, 2024) found that *CYP26A1*, but
69 not *FGF8*, is highly expressed in the developing macular region at day 40, after the onset of cone

genesis (corresponding to human ~PCW10(Hendrickson and Zhang, 2019)). However, little is known about the spatiotemporal expression of *CYP26A1* and *FGF8* in human fetal retina across the whole period of macular development. Moreover, while various roles have been ascribed to RA signaling across retinal development, the precise downstream functions of RA inhibition in human macular formation are not known.

Stem cell-derived human stem cell-derived retinal organoids (hROs) broadly resemble the human neural retina and closely follow the timing of human retinal development(Gonzalez-Cordero *et al.*, 2017). As such, they provide an opportunity to explore the signaling pathways that regulate human retinal development. Here, we used *in situ* hybridization in human fetal tissue and pharmacological manipulation in hROs to investigate the spatiotemporal expression and potential roles of RA and *FGF8* in human macular development.

82 # Results

83 **The RA catabolizing enzyme *CYP26A1* is expressed in two distinct waves within the**
84 **developing human macula**

85 To determine the spatiotemporal expression of *CYP26A1* and *FGF8,* we performed quantitative
86 RNAscope™ *in situ* hybridization on human fetal retina samples between PCW6 (CS16-17) and PCW17
87 (**Fig.1**). No distinct labelling for *CYP26A1* was visible anywhere in the retina at PCW6, but at PCW7
88 (CS18-19) weak, specific expression was just visible and localized to a single spot approximately 1mm
89 temporal to the optic nerve head (ONH) (**Fig.1a**), a location identified previously as the
90 PM(Hendrickson, 2016). Within this region, *CYP26A1* was distributed throughout the neuroblastic
91 layer (NBL), colocalizing with VSX2+ retinal progenitor cells (RPCs) (**Fig.1bi**).
92
93 At the start of PCW8 (CS20-21, herein termed "early PCW8"), significantly higher levels of *CYP26A1*
94 were observed in the PM within the VSX2+ NBL, compared to PCW7 ($q(15)=4.79$, $p=0.05$; **Fig.1a,bi,ci**),
95 with expression significantly reducing again by the end of PCW8 (CS22-23, herein termed "late PCW8";
96 $q(15)=6.34$, $p=0.006$; **Fig.1a,bi,ci**). *CYP26A1* was also expressed in the lens epithelium (LE) and at low
97 levels in the nasal edge of the retina and around the ONH at PCW7-early PCW8 (**Fig.1a; Fig.S1a**). To
98 provide context regarding retinal maturation, at late PCW8 RPCs expressing the cone/bipolar
99 progenitor marker OTX2 were distributed sparsely throughout the NBL of the entire retina, but were
100 more densely concentrated in the PM, where they were located towards the apical side of the retina
101 (**Fig.2ai-iv**). The RXRγ+ nascent GCL was visible throughout the retina, but only a few
102 RECOVERIN+/RXRγ+ cone photoreceptor cells were visible, in the PM (**Fig.2ai-ii**).
103

By PCW10, *CYP26A1* mRNA expression was significantly reduced in the PM region, compared to early PCW8 ($q(15)=7.28$, $p=0.002$; **Fig.1a,bi,ci**); moreover, its expression was restricted to a band of VSX2+/OTX2+ cells located in the nascent inner nuclear layer (INL) (**Fig.2bi-iv**), At PCW10, RXRγ+/RECOVERIN+/OTX2+ cone photoreceptors were located exclusively within a single cell layer (the nascent outer nuclear layer; ONL) at the apical edge of the PM, which did not express *CYP26A1* (**Fig.2bi-iv**). RXRγ+/RECOVERIN+ cones were not present in the peripheral retina at this stage (**Fig.2bi**).

At PCW12, *CYP26A1* expression was visibly increased within the PM, compared with PCW10, localizing to the basal edge of the VSX2+ INL, although this was not statistically significant (**Fig.1a,bi,ci**). However, by PCW17, expression of *CYP26A1* was significantly higher than PCW10 ($q(15)=9.71$, $p<0.0001$; **Fig.1a,bi,ci)** and PCW12 ($q(15)=7.23$, $p=0.002$; **Fig.1a,bi,ci; Fig.S1c**). At this stage, *CYP26A1* expression was exclusively within the PM (**Fig.1a**) and almost entirely restricted to VSX2+/SOX9+ MG cells, with minimal signal visible in the VSX2+/SOX9- bipolar cells or the ONL (**Fig.2c**).

Spatiotemporal *FGF8* expression pattern is not correlated with the human PM

In the chick, *Fgf8* is initially expressed in a comet-like pattern, with a broad stripe of lower expression extending temporally and a strong, central spot of expression overlapping with the spot-like expression of *Cyp26a1/c1* within the HAA(Silva and Cepko, 2017). In human fetal retina, positive *FGF8* mRNA labelling was visible around the ONH throughout PCW6-17 (**Fig.1a, Fig.S1a-b**), with the highest expression seen at PCW8 (**Fig.1bii,cii; Fig.3**). Examining the whole retina, expression exhibited a strong ONH-to-periphery gradient (**Fig.1a, Fig.3a, Fig.S1b**), similar to the developing macaque (d40)(Krueger *et al.*, 2024), mouse (E9.5-14.5)(Crossley and Martin, 1995),and chick eye (E2-E7)(Soukkarieh *et al.*, 2007), and from PCW12, *FGF8* labelling was also observed in the very peripheral retina, near the lens

127 (**Fig.1a**). However, in contrast to the clearly demarcated, spot-like and spatiotemporally coincident
128 expression of *Fgf8* and *Cyp26a1/c1* seen in the HAA of the chick, very little *FGF8* expression was
129 observed within the *CYP26A1*-positive PM (**Fig.1bi, Fig.S1a-b**). While some limited signal was
130 potentially discernible between PCW6-8 (**Fig.1cii**), this was not specific to the PM (**Fig.S1b**), and no
131 quantitatively significant differences in expression within the PM were detected between any
132 timepoints examined, including around periods of *CYP26A1* upregulation (PCW8/PCW17) (**Fig.1bi,ci**,
133 **Fig.S1a,c**).
134

135 **The PM is located more peripherally in early development, relative to its central position in**
136 **the mature retina, due to centre-to-periphery proliferation gradient**

137 In the adult eye, the macula is located at the center of the retina, approximately 3.5-5.5mm temporal
138 to the ONH(Bringmann *et al.*, 2018). At early developmental timepoints, however, the spot of *CYP26A1*
139 expression identified as the PM was more peripheral than expected (**Fig.1a**), prompting us to examine
140 growth and proliferation across regions of the retina throughout early development.
141

142 We measured the distance between the center of the region of *CYP26A1* expression (the PM) and i)
143 the peripheral edge of the retina; ii) the ONH (**Fig.4ai-iii**). The distance between PM-periphery
144 increased from 300µm to 9000µm between PCW7-17, growing in a linear manner (R^2=0.97; **Fig. 1a**,
145 **Fig.4aiv**). The distance from PM-ONH also grew in a linear manner, from 400µm to 6000µm (R^2=0.96;
146 **Fig.4aiv**), but the rate of increase was ~2-fold lower (890µm/week and 490µm/week, respectively,
147 p>0.001). Notably, while the distance PM-periphery increases as a proportion of total retina length,
148 from 20% at PCW7 to 45% at PCW17, PM-ONH remains constant at 30% (**Fig.4av**).

149

150 To determine whether this relative positional shift of the PM was the result of variable proliferation
151 across the retina, we examined regional proliferation using proliferative marker KI67 (**Fig.S2a**).
152 Consistent with the known center-to-periphery developmental gradient, and comparatively higher
153 proliferation in the periphery at later stages of retinal development(Hendrickson, 2016; Hoshino *et al.*,
154 2017), the proportion of Ki67+ cells was ~2-fold higher in the periphery compared to the central retina
155 at both early and late PCW8 (early PCW8: Peripheral 68%±11.6 vs Central 36%±3.4, late PCW8:
156 Peripheral 45%±19.1 vs Central 22%±3.7, respectively **Fig.4bi-ii**). The central-to-periphery proliferation
157 gradient thereby explains the more peripheral location of the PM at early stages, compared to the
158 adult eye (**Fig.4biii**).

159

160 **Reduction in proliferation marker KI67 in the PM coincides with *CYP26A1* expression at**
161 **PCW8**

162 We next examined proliferation within the PM during the first wave of *CYP26A1* expression, compared
163 to a region in the nasal retina equidistant from the periphery i.e. at the same position along on the
164 central-peripheral developmental gradient (**Fig.S2a**). As expected, both regions showed significant
165 reductions in the proportion of proliferating cells between PCW7 and early PCW8 (PM: $t(4)=6.5$,
166 $p=0.003$; nasal: $t(4)=5.0$, $p=0.007$; **Fig.4biv, Fig.S2b**). However, linear regression analysis showed that
167 the rate of reduction in the PM region was nearly twice that of the equivalent nasal region (-
168 31.2%/week and -17.3%/week, respectively, $p=0.046$) (**Fig.4biv, Fig.S2c**). This indicates that the
169 reduction in proliferation in the PM goes beyond that of the central-to-peripheral gradient; moreover,
170 this rapid reduction in proliferation in the PM coincides with the first wave of *CYP26A1* expression.

171

172 **hROs express components of RA synthesis and FGF8 pathways during early differentiation,**
173 **demonstrating similarity to peripheral retina development**

174 Our established 2D/3D differentiation protocol (**Fig.S3a**) replicates the timings of human development,
175 yielding hROs with ~1:4 ratio of cones:rods, a proportion similar to the outer edges of the
176 macula(Gonzalez-Cordero *et al.*, 2017). Note that this protocol includes the addition of exogenous RA
177 from d70, which is important for maintaining retinal structure in the later stages of
178 maturation(Sanjurjo-Soriano *et al.*, 2022) but by which time cone photoreceptor neurogenesis has
179 already occurred (**Fig.S3b-e**).
180
181 We examined the endogenous levels of RA and FGF8 signaling in our hROs. RA synthesizing enzymes,
182 *ALDH1A1* and *ALDH1A3,* were both upregulated early in differentiation (d40/50), compared to
183 undifferentiated hESCs ($q(2)=13.3$, $p=0.02$; $q(2)=23.2$, $p=0.005$; **Fig.5a,b**). CRABP2 traffics cytoplasmic
184 RA to the nucleus and is concomitantly upregulated with *all*-trans-RA, making it a proxy for circulating
185 RA levels(Napoli, 2016). *CRABP2* expression increased throughout differentiation, particularly beyond
186 d70, when exogenous RA is added ($q(2)=7.3$, $p=0.05$; **Fig.5c**). In contrast, *CYP26A1* expression was
187 lower in d40 hROs, compared to undifferentiated hESCs ($q(2)=15.4$, $p=0.01$) and remained low until
188 the addition of exogenous RA at d70, whereupon, unsurprisingly, it increased ($q(2)=8.0$, $p=0.04$) and
189 remained raised until d150 (**Fig.5d**).
190
191 *FGF8* was higher in d40 hROs compared to undifferentiated ESCs ($q(2)=18.02$, $p=0.008$), but expression
192 decreased thereafter (**Fig.5e**), whilst *FGFR3* was upregulated between d40-90, (reaching significance
193 at d50, $q(2)=10.2$, $p=0.02$), indicating FGF8 signaling is active over this period of hRO differentiation
194 (**Fig.5f**). Expression of *FGFR1/2/4* remained low throughout (**Fig.5f**).

195

196 **Early inhibition of RA by AGN193109 leads to smaller hROs and reduced proliferation**

197 Given the striking biphasic expression of *CYP26A1* within the human PM, we sought to mimic these
198 periods of reduced RA signaling in hROs to better understand their potential role(s) in macula
199 formation. In human fetal retina, the first wave of *CYP26A1* peaks in early PCW8, prior to RXRγ and
200 RECOVERIN protein expression (**Fig.2a**), which is equivalent to d40 in hROs (**Fig.S3e**). We therefore
201 attempted to recapitulate first wave of *CYP26A1*-induced RA catabolism by dosing hROs between d42-
202 50 ("early") with pan-RAR antagonist AGN193109 (10µM) (**Fig.S4a**)(Schubert and Germain, 2023).
203 Early dosing with AGN193109 significantly reduced expression of *CRABP2* ($t(2)=5.77$, $p=0.03$; **Fig.S5ai**)
204 and *CYP26A1* ($t(3)=7.91$, $p=0.004$; **Fig.S5ai**), demonstrating that this dose effectively reduced levels of
205 circulating RA. We also saw a concomitant significant increase in *FGF8* ($t(5)=5.51$, $p=0.003$; **Fig.S5aii**),
206 indicating RA activity has been successfully inhibited, resulting in activation of downstream
207 pathways(Cunningham and Duester, 2015).

208

209 Given the significant reduction in proliferation seen in the fetal PM during the first wave of *CYP26A1*
210 expression (**Fig.4biv**), we examined growth of hROs dosed with RA inhibitor AGN193109 to determine
211 whether RA inhibition reduced proliferation. Indeed, RA inhibition between d42-50 significantly
212 reduced growth by d60, compared with DMSO-treated controls ($t(32)=5.18$, $p<0.0001$), leading to
213 significantly smaller hROs at d150, following cessation of proliferation at 15 weeks(Gonzalez-Cordero
214 *et al.*, 2017) ($t(16)=2.66$, $p=0.017$) (**Fig.6a, Fig.S5b**). Quantification of proliferative marker KI67 also
215 showed a modest (~10%) but significant reduction in the proportion of KI67+ cells in AGN193109-
216 dosed hROs at d60, compared with DMSO-treated controls ($t(24)=2.48$, $p=0.02$) (**Fig.6bi**). Conversely,

217 there was no difference in the number of cells labelled with the apoptotic marker CASPASE-3
218 (t(29)=0.64, p=0.5) (**Fig.6bii**).
219

220 **Early pharmacological inhibition of RA signaling in hROs increases expression of**
221 **photoreceptor markers, while addition of recombinant FGF8 has no effect**

222 The data above suggests that, in keeping with previous studies which show RA regulates the balance
223 of proliferation and neurogenesis(Todd *et al.*, 2018), inhibition of RA between d42-50 promotes RPC
224 cell cycle exit in hROs. We therefore examined whether this earlier cell cycle exit increased the
225 adoption of early born cell fates. Indeed, we saw significantly increased expression of both pan-
226 photoreceptor marker *RECOVERIN* (t(5)=2.56, p=0.05) and cone progenitor maker *OTX2* (t(4)=4.58,
227 p=0.01) at d60 (**Fig.6ci**). The proportion of OTX2+ cells was also ~25% higher in early AGN193109-
228 dosed hROs than controls (t(28)=2.4, p=0.02) (**Fig.6d**). No significant changes were observed in the
229 expression of RPC marker *VSX2* (**Fig.6ci**,**d, Fig.S5di**), cone progenitor markers *RXRγ*/*THRβ* (**Fig.6ci,**
230 **Fig.S5dii**) or RGC marker *RBPMS* and RGC/bipolar/amacrine marker *ISLET1* (**Fig.S5ci-ii, diii**) by d60. We
231 also tested whether FGF8 signaling alters cone fate, as observed in chick, through addition of
232 recombinant (r)FGF8 (100ng/ml) between d42-50 (**Fig.S4b-c**) but saw no changes in RPC or
233 photoreceptor marker expression, compared with controls (**Fig.6cii**).
234

235 **Late RA inhibition results in decreased *S-OPSIN* and increased *M/L-OPSIN*, indicating a role**
236 **in cone subtype specification**

237 The data above indicates that the early wave of *CYP26A1* acts to promote cell cycle exit and the
238 acquisition of a cone progenitor fate. We next sought to additionally mimic the second, later wave of
239 *CYP26A1* expression. The "early+late" AGN193109 dosing protocol comprised of the "early" pulse at
240 d42-50, as above, and two later pulses, the first at d70-80, when RXRY/OTX2/RECOVERIN+ hRO cone
241 precursors have already been specified (**Fig.S3e**), equivalent to the start of the late *CYP26A1*
242 expression wave at PCW12 (**Fig.1, Fig.2b**), and the second at d120-130, when hRO cones have matured
243 and express *ARR3*, and rods express *RHODOPSIN* (**Fig.S3f-h**), equivalent to high *CYP26A1* expression at
244 PCW17 (**Fig.1, Fig.2c**). Note that we used two pulses, rather than sustained application, of AGN193109
245 in the later phase, as continuous removal of RA between d65-120 has previously been shown to cause
246 loss of stratification in hROs(Sanjurjo-Soriano *et al.*, 2022).
247
248 No change in pan-cone marker *ARRESTIN-3* or rod marker *RHODOPSIN* gene/protein expression was
249 observed at d150 with either early-only or early+late dosing (**Fig.7ai-ii, bi-ii**), indicating the overall
250 proportions of cones and rods were not affected. However, those receiving early+late dosing showed
251 a significant 2-fold reduction of *S-OPSIN* ($t(5)=6.68$, $p=0.001$) and a concurrent, significant ~4-fold
252 increase in *L-OPSIN* ($t(5)=3.27$, $p=0.02$) and ~2-fold increase in *M-OPSIN* ($t(5)=1.53$, $p=0.04$), compared
253 to DMSO controls (**Fig.7aiii-v**). Conversely, hROs receiving early-only dosing showed no changes in
254 cone subtype marker expression at d150 (**Fig.7aiii-vi)**. Immunostaining analysis revealed that
255 early+late dosing with AGN193109 led to a significant reduction in the proportion of ARR3+ cones
256 expressing S-OPSIN protein ($t(11)=3.14$, $p=0.01$) (**Fig.7biii,v**), although we did not observe a change in
257 the proportion of M/L-OPSIN/ARR3+ cones (**Fig.7biv,vi**). These results indicate that inhibition of RA
258 signaling later in cone development alters cone subtype specification.

Discussion

Analysis of early-stage human macular development has been very limited to date, in particular prior to PCW8, with small sample sizes due to scarcity. The earliest previous *in situ* spatial analysis of *CYP26A1* expression in human fetal retina was late PCW8 (CS22-23), which showed expression in the PM at CS22 but none at CS23(Silva and Cepko, 2017). Here, we provide the first spatiotemporal developmental timeline of *CYP26A1* expression in the developing human macula, revealing a striking biphasic pattern of expression. Importantly, we show that the first wave of *CYP26A1* expression is initiated in the RPCs of the PM at PCW7, prior to cone genesis, and is already reducing by late PCW8, while the second wave is evident from PCW12 and is specific to the MG within the INL of the PM. This second wave in the MG layer is in line with transcriptomic studies on adult human retina(Peng *et al.*, 2019; Cowan *et al.*, 2020), as well as a recently published single-nuclei gene expression data of PCW8-23 fetal retina, which showed *CYP26A1* was highly enriched in PCW17 macula cells(Zuo *et al.*, 2024). Our findings are also consistent with a recent report of *CYP26A1* expression in rhesus macaque development(Krueger *et al.*, 2024), which presented strong, biphasic *CYP26A1* expression in the PM region(Hendrickson and Zhang, 2019). In both human and macaque, *CYP26A1* was only expressed in RPCs during early macular formation, with no *CYP26A1* mRNA observed in the OTX2+/RXRγ+/RECOVERIN+ cone precursor cells of the ONL, indicating that RA inhibition may play a role in progenitor cell differentiation.

In contrast to HAA formation in the chick, where there is a striking spatiotemporal pattern of *Fgf8* expression in the HAA, we saw no indications of focal *FGF8* expression specific to the *CYP26A1+* PM. Instead, *FGF8* expression remained low and exhibited no significant changes in expression in the human PM throughout PCW6-17 of development. Specifically, *FGF8* was not upregulated following

282 *CYP26A1* expression in the PM at PCW8, in contrast to the chick HAA(da Silva and Cepko, 2017),
283 suggesting additional/different regulatory mechanisms downstream of *CYP26A1* and low RA in the
284 human macula. These findings are consistent with recent human fetal single-nuclei gene expression
285 data, which found *FGF8* was enriched in peripheral, but not macula, RPCs(Zuo *et al.*, 2024), and
286 RNAscope analysis of rhesus macaque development, where *FGF8* was not enriched in the developing
287 macula region at any timepoint examined(Krueger *et al.*, 2024). Moreover, we found addition of rFGF8
288 to hRO cultures had no impact on photoreceptor marker expression. These suggest that *FGF8* is
289 unlikely to play a significant role in human macula formation or macula cone differentiation. They also
290 indicate a degree of divergence in the molecular mechanisms underlying high-acuity region
291 development in different species and particularly warrant further investigation into the pathways
292 downstream of *CYP26A1* in the human retina.
293
294 RPC differentiation and maturation occurs earlier in the macula than the rest of the retina, shown
295 previously by primate and human studies(Vail, Rapaport and Rakic, 1991; Hendrickson, 1992; Provis
296 and Hendrickson, 2008; Lu *et al.*, 2020; Sridhar *et al.*, 2020). Whilst peripheral RPCs have been shown
297 to maintain their progenitor state for longer than those in the PM, and higher rates of proliferation are
298 observed in the periphery from PCW8(Hendrickson, 2016; Hoshino *et al.*, 2017), earlier region-specific
299 differences have not been studied due to lack of markers and access to tissue. Previously, bulk retina
300 RNAseq showed enrichment of proliferation-related genes between PCW7-10, and
301 immunohistochemistry showed reduced KI67 expression in the central compared to peripheral retina
302 at PCW8(Hoshino *et al.*, 2017). Developing this further, we found that there is a marked reduction in
303 proliferation specifically within the PM at early PCW8 (CS20-21), coincident with the first wave of
304 *CYP26A1* expression. Given the known role of RA in maintaining the cell cycle(Kam *et al.*, 2012), this
305 first wave of *CYP26A1* appears to serve to promote early cell cycle exit within the PM.

306

307 We investigated *CYP26A1's* roles in human macular development by inhibiting RA signaling in hROs via
308 pharmacological blocking of RARs to mimic the low RA environment of the *CYP26A1+* PM. Given the
309 coincident expression of *CYP26A1* and reduced proliferation in PCW7-8 PM, we asked whether early
310 inhibition of RA encourages cell cycle exit and neurogenesis. Indeed, we observed significantly fewer
311 proliferating cells and reduced growth in hROs exposed to early RAR inhibition, leading to significantly
312 smaller hROs at both d60 and d150. This aligns with our previous data investigating the effects of
313 exogenous RA on mouse ESC-derived retinal organoids (mROs), where the inverse occurs, and a short
314 pulse of RA from d14-16 (cone precursor stage) led to an increase in proliferation and overall cell
315 yield(Kruczek *et al.*, 2017). In the current study, early-dosed hROs also displayed a significant increase
316 in the number of OTX2+ cells at d60, consistent with early cell cycle exit leading to differentiation of
317 early-born cell types in the forming macula. However, this increase at d60 was not reflected in a
318 concomitant increase at d150, presumably because supplementary pathways not active in the culture
319 system, such as ONECUT1-mediated induction of thyroid signaling factors(Emerson *et al.*, 2013; Eldred
320 *et al.*, 2018), are required for complete maturation into adult cones in hROs. Similarly, while the
321 upregulation of *FGF8* in response to early RA-inhibition in hROs (Fig.S5aiii) is consistent with RA's
322 known role in inhibiting *Fgf8* expression(Cunningham and Duester, 2015), it implies that in the human
323 macula itself additional regulatory mechanisms may act to prevent *FGF8* upregulation in response to
324 low RA concentration.

325

326 Additional pulses of RA inhibition, aimed at mimicking the second wave of *CYP26A1* expression, did
327 not lead to a change in overall proportions of cones:rods in mature hROs, despite RA being known to
328 promote rod production(Osakada *et al.*, 2008), and removal of RA leading to more cone-rich
329 organoids(Sanjurjo-Soriano *et al.*, 2022). This may be because a more sustained period of low RA is

330 required for a shift towards cone-rich hRO, since *in vivo CYP26A1* expression increases from PCW12
331 onwards and remains elevated for many weeks. As noted earlier, however, we did not try to replicate
332 this since continuous removal of RA between d65-120 has previously been shown to cause loss of
333 stratification in hROs(Sanjurjo-Soriano *et al.*, 2022).
334
335 Cone subtypes are determined by two fate check points: first, between S or M/L fate, and if the latter,
336 between M- or L-OPSIN expression. The foveola at the center of the macula contains only M/L-cones
337 while S-cones are present in the periphery of the retina. S-OPSIN-expressing cones are initially present
338 in the early PM, and it is hypothesized that they later convert to M/L-cones, indicating plasticity of
339 cone fate(Xiao and Hendrickson, 2000; Cornish *et al.*, 2004). When RA signaling was inhibited early in
340 differentiation, prior to cone neurogenesis, we observed no change in cone subtypes at d150.
341 However, the addition of a later period of RA signaling inhibition led to a significant upregulation of
342 *M/L-OPSIN* and concomitant downregulation of *S-OPSIN* gene expression and fewer S-OPSIN+ cells.
343 This reflects a recent BioRxiv report showing that *CYP26A1*-null hROs favor S-cone formation(Hussey
344 *et al.*, 2023). Interestingly, a similar effect was seen in *VAX2* knockout mice; normally *VAX2* restricts
345 the expression of *CYP26A1* to a stripe in the central retina. In its absence, there is an expansion of M-
346 cones into the usually S-cone dominated ventral retina(Alfano *et al.*, 2011). Moreover, addition of
347 exogenous RA to mROs after the period of cone precursor specification led to upregulation of S-opsin
348 but no change in Arrestin-3 expression, indicating that alterations in RA signaling later in development
349 also influence S- vs M/L-opsin cone subtype specification in mouse development(Kruczek *et al.*, 2017).
350
351 RA has also recently been shown to regulate the M- vs L-cone cell fate(Hadyniak *et al.*, 2024). In our
352 hands, while the addition of late pulses of RA inhibition in hROs led to an increase in both *M-* and *L-*
353 *OPSIN* expression, we saw a greater impact on *L-OPSIN* expression, compared to *M-OPSIN* (~4-fold,

354 versus ~2-fold, increase respectively), indicating that lack of RA signaling more strongly favors L-cone
355 fate. This broadly aligns with a recent report by Johnston and colleagues indicating that sustained
356 application of RA to hROs during the same period of differentiation (d43-d130) of RA suppresses L-
357 cone formation, whilst promoting M-cone fate(Hadyniak *et al.*, 2024).
358
359 Together, these data show for the first time the spatiotemporal biphasic pattern of expression of
360 *CYP26A1* within the PM across human macula development. Conversely, *FGF8* expression shows no
361 such spatiotemporal changes in the PM, consistent with the macaque but in contrast to the chick HAA,
362 suggesting a divergence of regulatory mechanisms in high-acuity area formation. Based on our analysis
363 of RA pathway manipulation in hRO models, we propose different roles for the two waves of CYP26A1-
364 mediated RA inhibition in macular formation: the early wave (PCW7-8) stimulates RPCs to exit the cell
365 cycle, encouraging cone generation, while the second, later wave (from PCW12) plays a role in the
366 specification of cone subtypes.
367
368 This work bridges a gap in fundamental knowledge of the molecular mechanisms underlying human
369 macular development and highlights the importance (and challenges) of studying human development
370 in both animal models and human-derived tissue. These results open new avenues for future research
371 including resolving the molecular network downstream of *CYP26A1* and determining the drivers of
372 *CYP26A1* expression in the human PM and how they are initiated. Elucidating these molecular
373 mechanisms could provide strategies to encourage formation of more macular-like cellular structure
374 in *in vitro* models to study macular development and disease, provide a preclinical model for drug
375 testing to treat macular degeneration, and improve the efficacy of generating cells used for
376 transplantation therapies that to restore visual function in patients.

377 # Experimental Procedures

378 ## Human fetal retina sample collection

379 Human fetal retina samples were collected from the Human Developmental Biology Resource with
380 research ethics approval and informed consent (Project 200599, REC 18/LO/0822 and 18/NE/0290,
381 IRAS: 244325 and 250012). Samples were stored in compliance with the Human Tissue Act 2004.
382 Staging was performed by the HDBR according to defined criteria (https://hdbratlas.org/staging-
383 criteria/carnegie-staging.html). A minimum of 2 biological replicates from independent samples were
384 analyzed for each timepoint.

385 ## Differentiation of retinal organoids

386 Cells from the H9 ESC line were maintained and used to generate human retinal organoids (hROs)
387 according to a previously published protocol(Gonzalez-Cordero *et al.*, 2017). Full protocol and reagents
388 can be found in supplementary material. For dosing, 10µM AGN193019 (Bioteche: 5758) or 100ng/µl
389 rFGF8 (Biotechne: 423-F8-025) were added to culture media every 2 days throughout the dosing
390 windows.

391 ## RNAscope™ *in situ* hybridization

392 RNAscope™ Multiplex Fluorescence Assay was performed using manufacturer's protocol for fixed
393 frozen tissue with manual antigen retrieval. Sections were incubated with catalogue probes Hs-
394 CYP26A1-C1 (ACD Bio: 487741) and Hs-FGF8-C2 (ACD Bio: 415791-C2), counterstained with VSX2 and
395 DAPI. Full protocol, reagents and quantification can be found in supplementary material.

396 **Immunohistochemistry (IHC)**

397 IHC was performed using primary/secondary antibodies listed in **Table S1**/**S2**. Full protocol, reagents
398 and quantification can be found in supplementary material.

399 **qRT-PCR gene expression analysis**

400 qRT-PCR was performed to analyze gene expression using primers listed in **Table S3**. Full protocol,
401 reagents and quantification can be found in supplementary material.

402 **Fetal retina regional distance measurements**

403 Regional length measurements were taken from confocal RNAscope™ images with fluorescent
404 *CYP26A1* staining. The outer edge of the retina was manually traced using the segmented line drawing
405 tool in ImageJ, from the center of *CYP26A1* expression (white arrow, Fig.4a) to the peripheral edge, or
406 edge of optic stalk, and distance calculated using the measure function. Growth rates were analyzed
407 using linear regression analysis in GraphPad Prism (v10.1.2).

408 **Statistics**

409 All data are presented as mean±SD; N denotes number of independent experiments (i.e.,
410 differentiation batches) and n denotes number of images or hROs examined. Statistical testing was
411 performed in GraphPad Prism (version 10.1.2). Tests used to analyze statistical significance are
412 specified in methods/figure legends. Outliers were identified and excluded using the ROUT test
413 (Q=10%). Shapiro-Wilk Tests were used to assess normality and F-tests were used to confirm equal
414 variances prior to applying parametric statistical tests.

Resource Availability

Further information and requests for resources/reagents should be directed to the corresponding authors.

Materials Availability

This study did not generate new unique reagents.

Data and Code Availability

This paper did not generate original code. Additional data is available from the corresponding authors upon request. FAIR data management principles were followed throughout.

Acknowledgements

This research was funded by Fight for Sight (5139/5140) and Medical Research Council UK (MR/T002735/2). Maja Wojtynska was funded by the Wellcome Trust as part of the Advanced Therapies for Regenerative Medicine Wellcome Trust PhD Program (218461/Z/19/Z). This work was made possible by the support, dedication and teamwork of the Ocular Cell and Gene Therapy team, with particular thanks to Dr E West, Dr M Branch, Dr M Khazim, B Ladino, J Kapadia, E Lanning, M Margari, M Tariq, C Mofidi, K Kumar, S Guilfoyle, S van Heerden for help with stem cell maintenance cultures. We wish to thank Dr M Riabiz (KCL) for providing independent expert statistical analysis advice. For the purpose of open access, the authors have applied a Creative Commons Attribution (CC BY) license to any Author Accepted Manuscript version arising. Graphical images were created in BioRender.

Author Contributions

Conceptualization – PH, RP; Data curation – PH, MW; Formal Analysis – PH; Funding acquisition – RP; Investigation – PH, RP; Methodology – PH, RP; Supervision – RP; Visualization – PH; Writing – original draft – PH; Writing – review & editing – PH, AS, RA, RP

Declaration of Interests

The authors declare no competing interests.

441 # References

442 Alfano, G. *et al.* (2011) 'Vax2 regulates retinoic acid distribution and cone opsin expression in the
443 vertebrate eye', *Development*, 138(2), pp. 261–271. doi: 10.1242/DEV.051037.

444 Bringmann, A. *et al.* (2018) 'The primate fovea: Structure, function and development', *Progress in*
445 *Retinal and Eye Research*, 66, pp. 49–84. doi: 10.1016/j.preteyeres.2018.03.006.

446 Cornish, E. E. *et al.* (2004) 'The role of opsin expression and apoptosis in determination of cone types
447 in human retina', *Experimental Eye Research*, 78(6), pp. 1143–1154. doi: 10.1016/J.EXER.2004.01.004.

448 Cowan, C. S. *et al.* (2020) 'Cell Types of the Human Retina and Its Organoids at Single-Cell Resolution',
449 *Cell*, 182(6), pp. 1623-1640.e34. doi: 10.1016/j.cell.2020.08.013.

450 Crossley, P. H. and Martin, G. R. (1995) 'The mouse Fgf8 gene encodes a family of polypeptides and is
451 expressed in regions that direct outgrowth and patterning in the developing embryo', *Development*,
452 121(2), pp. 439–451. doi: 10.1242/DEV.121.2.439.

453 Cunningham, T. J. and Duester, G. (2015) 'Mechanisms of retinoic acid signalling and its roles in organ
454 and limb development', *Nature Reviews Molecular Cell Biology*, 16(2), pp. 110–123. doi:
455 10.1038/nrm3932.

456 Curcio, C. A. *et al.* (1990) 'Human photoreceptor topography', *The Journal of Comparative Neurology*,
457 292(4), pp. 497–523. doi: 10.1002/CNE.902920402.

458 Cvekl, A. and Wang, W.-L. L. (2009) 'Retinoic acid signaling in mammalian eye development',
459 *Experimental Eye Research*, 89(3), pp. 280–291. doi: 10.1016/j.exer.2009.04.012.

460 Eldred, K. C. *et al.* (2018) 'Thyroid hormone signaling specifies cone subtypes in human retinal
461 organoids', *Science*, 362(6411). doi: 10.1126/SCIENCE.AAU6348.

462 Emerson, M. M. *et al.* (2013) 'Otx2 and Onecut1 promote the fates of cone photoreceptors and
463 horizontal cells and repress rod photoreceptors', *Developmental cell*, 26(1), pp. 59–72. doi:

464 10.1016/J.DEVCEL.2013.06.005.

465 Gonzalez-Cordero, A. *et al.* (2017) 'Recapitulation of Human Retinal Development from Human
466 Pluripotent Stem Cells Generates Transplantable Populations of Cone Photoreceptors', *Stem Cell*
467 *Reports*, 9(3), pp. 820–837. doi: 10.1016/j.stemcr.2017.07.022.

468 Hadyniak, S. E. *et al.* (2024) 'Retinoic acid signaling regulates spatiotemporal specification of human
469 green and red cones', *PLoS biology*, 22(1), p. e3002464. doi: 10.1371/JOURNAL.PBIO.3002464.

470 Hendrickson, A. (1992) 'A morphological comparison of foveal development in man and monkey', *Eye*,
471 6(2), pp. 136–144. doi: 10.1038/eye.1992.29.

472 Hendrickson, A. (2016) 'Development of Retinal Layers in Prenatal Human Retina', *American Journal*
473 *of Ophthalmology*, 161, pp. 29–35. doi: 10.1016/J.AJO.2015.09.023.

474 Hendrickson, A. and Zhang, C. (2019) 'Development of cone photoreceptors and their synapses in the
475 human and monkey fovea', *The Journal of Comparative Neurology*, 527(1), pp. 38–51. doi:
476 10.1002/CNE.24170.

477 Hoshino, A. *et al.* (2017) 'Molecular Anatomy of the Developing Human Retina', *Developmental Cell*,
478 43(6), pp. 763–779. doi: 10.1016/J.DEVCEL.2017.10.029.

479 Hussey, K. *et al.* (2023) 'Foveolar cone subtype patterning in human retinal organoids', *bioRxiv*. doi:
480 10.1101/2023.01.28.526051.

481 Kam, R. K. T. *et al.* (2012) 'Retinoic acid synthesis and functions in early embryonic development', *Cell*
482 *& Bioscience*, 2(1), pp. 1–14. doi: 10.1186/2045-3701-2-11.

483 Kruczek, K. *et al.* (2017) 'Differentiation and Transplantation of Embryonic Stem Cell-Derived Cone
484 Photoreceptors into a Mouse Model of End-Stage Retinal Degeneration', *Stem Cell Reports*, 8(6), pp.
485 1659–1674. doi: 10.1016/j.stemcr.2017.04.030.

486 Krueger, M. R. *et al.* (2024) 'Expression patterns of CYP26A1, FGF8, CDKN1A, and NPVF in the
487 developing rhesus monkey retina', *Differentiation*, 135, p. 100743. doi: 10.1016/J.DIFF.2023.100743.

488 Lahne, M., Yoshimatsu, T. and MacDonald, R. B. (2023) 'Retinoic acid signaling in the developing
489 zebrafish high acuity zone', *Investigative Ophthalmology & Visual Science*, 64(8), pp. 3630–3630.
490 Lu, Y. *et al.* (2020) 'Single-Cell Analysis of Human Retina Identifies Evolutionarily Conserved and
491 Species-Specific Mechanisms Controlling Development', *Developmental Cell*, 53(4), pp. 473–491. doi:
492 10.1016/j.devcel.2020.04.009.
493 Mey, J. and Thanos, S. (2000) 'Development of the visual system of the chick: I. Cell differentiation and
494 histogenesis', *Brain Research Reviews*, 32(2–3), pp. 343–379. doi: 10.1016/S0165-0173(99)00022-3.
495 Napoli, J. L. (2016) 'Functions of Intracellular Retinoid Binding-Proteins', *Sub-cellular Biochemistry*, 81,
496 pp. 21–76. doi: 10.1007/978-94-024-0945-1_2.
497 Osakada, F. *et al.* (2008) 'Toward the generation of rod and cone photoreceptors from mouse, monkey
498 and human embryonic stem cells', *Nature Biotechnology*, 26(2), pp. 215–224. doi: 10.1038/nbt1384.
499 Peng, Y. R. *et al.* (2019) 'Molecular Classification and Comparative Taxonomics of Foveal and Peripheral
500 Cells in Primate Retina', *Cell*, 176(5), pp. 1222–1237. doi: 10.1016/J.CELL.2019.01.004.
501 Provis, J. M. and Hendrickson, A. E. (2008) 'The Foveal Avascular Region of Developing Human Retina',
502 *Archives of Ophthalmology*, 126(4), pp. 507–511. doi: 10.1001/ARCHOPHT.126.4.507.
503 Sanjurjo-Soriano, C. *et al.* (2022) 'Retinoic acid delays initial photoreceptor differentiation and results
504 in a highly structured mature retinal organoid', *Stem Cell Research & Therapy*, 13(1), pp. 1–17. doi:
505 10.1186/S13287-022-03146-X.
506 Schubert, M. and Germain, P. (2023) 'Retinoic Acid and Retinoid X Receptors', *Cells*, 12(6), p. 864. doi:
507 10.3390/CELLS12060864.
508 Silva, S. da and Cepko, C. L. (2017) 'Fgf8 Expression and Degradation of Retinoic Acid Are Required for
509 Patterning a High-Acuity Area in the Retina', *Developmental Cell*, 42(1), pp. 68–81. doi:
510 10.1016/j.devcel.2017.05.024.
511 Soukkarieh, C. *et al.* (2007) 'Pax2 regulates neuronal–glial cell fate choice in the embryonic optic

512 nerve', *Developmental Biology*, 303(2), pp. 800–813. doi: 10.1016/J.YDBIO.2006.11.016.

513 Sridhar, A. *et al.* (2020) 'Single-Cell Transcriptomic Comparison of Human Fetal Retina, hPSC-Derived
514 Retinal Organoids, and Long-Term Retinal Cultures', *Cell Reports*, 30(5), pp. 1644–1659. doi:
515 10.1016/j.celrep.2020.01.007.

516 Todd, L. *et al.* (2018) 'Retinoic Acid-Signaling Regulates the Proliferative and Neurogenic Capacity of
517 Müller Glia-Derived Progenitor Cells in the Avian Retina', *Stem cells*, 36(3), pp. 392–405. doi:
518 10.1002/STEM.2742.

519 Vail, M. M. la, Rapaport, D. H. and Rakic, P. (1991) 'Cytogenesis in the monkey retina', *Journal of*
520 *Comparative Neurology*, 309(1), pp. 86–114. doi: 10.1002/CNE.903090107.

521 Voigt, A. P. *et al.* (2021) 'Human photoreceptor cells from different macular subregions have distinct
522 transcriptional profiles', *Human molecular genetics*, 30(16), pp. 1543–1558. doi:
523 10.1093/hmg/ddab140.

524 Xiao, M. and Hendrickson, A. (2000) 'Spatial and temporal expression of short, long/medium, or both
525 opsins in human fetal cones.', *The Journal of Comparative Neurology*, 425(4), pp. 545–559.

526 Zuo, Z. *et al.* (2024) 'Single cell dual-omic atlas of the human developing retina', *Nature*
527 *Communications*, 15(1), pp. 1–21. doi: 10.1038/s41467-024-50853-5.

528

Figures

Fig.1. *CYP26A1* shows focal, biphasic expression within the PM of PCW6-17 human fetal retina, peaking at early PCW8 and PCW16/17. (a) Human fetal retina samples from PCW6-17 stained for *FGF8* *(*cyan) and RA catabolizing enzyme *CYP26A1* (magenta), showing *CYP26A1*+ spot-like PM region colocalizing with RPC (retinal progenitor cell) marker, VSX2 (green) in the neuroblastic layer between PCW7-8 (CS18-23), and basal to the VSX2+ layer at PCW12-17. (b) Zoom-ins of the (i) PM and (ii) ONH, (c) Quantification of *CYP26A1*/*FGF8* fluorescence intensity over PCW6-17 in PM/ONH, normalized to positive control (*POLR2A*/*PPIB*). One-way ANOVA yielded a statistically significant difference in *CYP26A1* expression in the PM between at least 2 timepoints ($F(6,15)=13.96$, $p<0.0001$), and Tukey's test found significant increase in mean fluorescence intensity between PCW7-early PCW8 (CS20-21) ($q(15)=6.34$, $p=0.006$), and a significant decrease between early PCW8-late PCW8 (CS22-23) ($q(15)=5.90$, $p=0.01$). ANOVA found statistical differences in *CYP26A1* expression in the ONH ($F(6,14)=3.39$,$p=0.03$), however, no significance was identified by post-hoc tests. ANOVA yielded no significant differences in *FGF8* expression in the PM ($F(6,15)=1.18$,$p=0.40$) between any time points. Conversely, statistical differences were found in *FGF8* in the ONH ($F(6,15)=4.06$,$p=0.01$), with significantly higher *FGF8* at PCW8 compared to PCW12 ($q(15)=5.45$, $p=0.02$) and PCW17 ($q(15)=4.95$, $p=0.04$). Images of probe labelling through entire CS20 retina, positive and negative controls, intensity measurements and all multiple comparison results for PM *CYP26A1* expression are shown in **Fig.S1**. White arrows indicate PM, while white outlined arrow heads indicate low levels of *CYP26A1* expression visible at nasal edge of the retina. Sections counterstained with DAPI (greyscale). T: Temporal; N: Nasal; CS: Carnegie Stage; PCW: Post-conception Weeks, PM: Presumptive macula. *p value<0.05, **p value<0.01, *** p value<0.001. Data shown as mean±SD. Images taken at (a) 20x/(b) 40x, representative of n≥2 samples/timepoint. Scale bars: (a) 500μm, (b) 100μm.

552 **Fig.2. Cone progenitor markers are expressed in the NBL of late PCW8 PM, localized to the INL by**
553 **PCW10 but do not co-express *CYP26A1*, while macular Müller Glia (MG) cells express *CYP26A1* in**
554 **PCW17 human fetal retina.** (a), At late PCW8 (CS23), OTX2 (yellow) is expressed in cone/bipolar-biased
555 RPCs in the neuroblastic layer (NBL) throughout the retina, at highest density in the PM, while no
556 RECOVERIN (red) or RXRγ+ (cyan) cone precursor markers are visible. (b), At PCW10, the PM region
557 expresses a thick layer of OTX2+ cells in the INL, and RXRγ+/RECOVERIN+ cone precursors localize to
558 the apical single-cell thick ONL layer of the central retina, not present in the peripheral retina. *CYP26A1*
559 expression is restricted to the INL, not expressed in the RECOVERIN+/RXRγ+/OTX2+ cone precursors in
560 the ONL. (c) At PCW17, *CYP26A1* (magenta) is visible in the PM, localized to the VSX2+ (green)/SOX9+
561 (yellow) developing Müller glia layer, basal to the VSX2+/SOX9- developing bipolar cell layer. Müller
562 glia cytoskeletal marker Vimentin (VIM, red) is clearly expressed, while no *FGF8* (cyan) is visible in the
563 PM. Stains were performed on consecutive sections from the same respective retina for ai/iii, bi/iii and
564 ci/ii, and counterstained with DAPI (greyscale). CS: Carnegie Stage; PCW: Post-conception Weeks; NBL:
565 Neuroblastic Layer; GCL: Ganglion Cell Layer; ONL: Outer Nuclear Layer; INL: Inner Nuclear Layer.
566 Images taken at (ai/bi) 20x/(aii-iii/bii-iii/c) 40x. White box indicates magnified region of interest.
567 Images representative of n≥2 samples. Scale bars: (a) 500μm, (b-c) 100μm.
568
569 **Fig.3. *CYP26A1* is highly expressed in the PM of early PCW8 (CS20) human fetal retina, while *FGF8* is**
570 **localized exclusively to the optic nerve head (ONH).** Early PCW8 (CS20) fetal retina stained *in situ* for
571 *CYP26A1* (magenta) and *FGF8* (cyan), showing strong expression in the PM of *CYP26A1* colocalizing
572 with RPC marker VSX2 (green), but no *FGF8*, which is visible in RPCs around the ONH. Assay negative
573 control (*DapB*) and positive control (*PPIB* cyan, *POLR2A* magenta). Sections counterstained with DAPI
574 (greyscale). T: Temporal; N: Nasal; CS: Carnegie Stage; PCW: Post-conception Weeks; PM: Presumptive

575 Macula; ONH: Optic Nerve Head. Images taken at 20x (b)/40x (a). Images representative of n=3
576 samples. White box indicates magnified region of interest. Scale bars: (a) 500μm, (b) 100μm.
577
578 **Fig.4. Higher proliferation in peripheral compared to central retina results in a temporally shifted**
579 ***CYP26A1*+ PM at early developmental stages (PCW7-10).** (a), (i-iii) The distance of the *CYP26A1*+
580 (magenta) PM (white arrow) to the peripheral edge of the retina/ONH. (iv) PM-periphery distance
581 increases at a significantly higher rate (>2-fold) between PCW7-17 compared with PM-ONH distance,
582 $p<0.001$. (v) The PM-periphery distance as a proportion of the whole retina increases from 20%-45%
583 over PCW7-17, while PM-ONH distance remains almost constant at 30% of the whole retina (n=14,
584 linear regression with 95% confidence internals plotted). (b) (i) Representative images of proliferative
585 marker KI67 (yellow) staining in PCW7-8 (CS18-23) human fetal retinas shows: (ii) the proportion of
586 DAPI+ (grey) cells expressing KI67 was at ~two-fold higher in the peripheral compared with central
587 retina during PCW7-8 (PCW7: $t(2)=3.3$, $p=0.08$; early PCW8 (CS20): $t(2)=6.4$, $p=0.02$; late PCW8 (CS23):
588 $t(2)=2.5$, $p=0.13$). (iii) Schematic showing centre-to-periphery proliferation gradient, and the
589 peripheral location of the PM in early development gradually moving towards the centre of the retina
590 due to higher relative growth at the peripheral edge. (iv) Linear regression shows the decline in
591 KI67+/DAPI+ cells in the PM region is significantly steeper than the nasal region between PCW7 and
592 early PCW8, at which point *CYP26A1* is upregulated in the PM (PM: -32.2, nasal: -17.3, $p=0.046$). Region
593 masking and full linear regression shown in **Fig.S2**. Significance values determined by paired/unpaired
594 t-tests: *p value<0.05, **p value<0.01. n=3 samples/timepoint, data shown as mean±SD. PCW: Post-
595 conception Weeks; CS: Carnegie Stage; PM: Presumptive Macula, ONH: Optic Nerve Head. Images
596 taken at 20x. Scale bars: (a) 500μm, (b) 100μm.
597

598 **Fig.5. Differentiating human retinal organoids express retinoic acid and FGF8 pathway components**.
599 (a) Relative expression of RA synthesizing enzymes across hRO differentiation showing significant
600 upregulation of *ALDH1A1* from d40 ($q(2)=13.3$, $p=0.02$), and *ALDH1A3* from d50 ($q(2)=23.2$, $p=0.005$).
601 (b) Immunostaining of ALDH1A1 and ALDH1A3 in d40 hROs showing expression throughout the
602 organoid, co-stained with neural retinal progenitor cell marker VSX2, counterstained with DAPI (blue).
603 (c-f) Relative expression of mRNA for: (c) proxy for circulating RA levels *CRABP2,* with expression
604 increasing from d40, but significantly upregulated at d80, following exogenous RA addition ($q(2)=7.3$,
605 $p=0.05$); (d) retinoic acid catabolizing enzyme *CYP26A1*, initially downregulated compared to hESCs
606 ($q(2)=15.4$, $p=0.01$), but upregulated at d80 following standard protocol addition of exogenous RA to
607 culture medium from d70 ($q(2)=8.0$, $p=0.04$); (e) fibroblast growth factor 8 (*FGF8*), which has
608 significantly increased expression at d40 ($q(2)=18.02$, $p=0.008$) and expression remains high, although
609 slowly decreases up to d90; and (f) FGF receptors (*FGFR1/2/3/4*), which all showed slight
610 downregulation compared to hESCs (*FGFR1* d60: $q(2)=14.1$, $p=0.01$; *FGFR4* d90: $q(2)=8.2$, $p=0.04$),
611 except *FGFR3* which was significantly upregulated at d50 ($q(2)=10.2$, $p=0.02$), with expression
612 remaining high, although slightly decreasing to d90. Further hRO marker expression shown in **Fig.S3**.
613 qPCR data shown as Log_2 fold change of CT values relative to d0 hESCs (n=5 pooled hROs/sample, N=3).
614 Significance values determined by one-way repeated measures ANOVA followed by Dunnett's test
615 against control group, adjusting for multiple comparisons: *p value<0.05, **p value<0.01, ***p
616 value<0.001, data shown as mean±SD. Staining images representative of n=3 hROs from N=1 batch.
617 Scale bars: 100μm.
618
619 **Fig.6. Dosing early hROs with RA receptor inhibitor AGN193109 results in reduced proliferation and**
620 **increased cone precursor marker OTX2 expression.** (a) Following dosing between d42-50 ("early"),
621 the % change in area from d42-d60 was found to be significantly lower in AGN193109 dosed hROs

622 compared with DMSO dosed controls, demonstrating reduced growth in RA inhibited hROs
623 (t(32)=5.18, p<0.0001). (b), Immunostaining for (i) apoptotic marker CASPASE-3 (yellow) at d60 showed
624 no significant increase in cell death between AGN193109 dosed and control hROs (t(29)=0.64, p=0.5),
625 (ii) proliferative marker KI67 (green) showed a significant reduction in cell proliferation in RA inhibited
626 hROs (t(24)=2.48, p=0.02). (c) (i) Dosing with AGN193109 led to significant increases in photoreceptor
627 marker *RECOVERIN* (t(5)=2.56, p<0.05), and cone progenitor marker *OTX2* (t(4)=4.58, p=0.01), while
628 early cone precursor markers *RXR*γ and *THR*β trended towards increased expression (t(5)=1.45,
629 p=0.2)/(t(5)=1.69, p=0.15), with no increase in retinal progenitor cell (RPC) marker *VSX2* (t(5)=1.39,
630 p=0.2). (ii) Dosing with rFGF8 had no effect on any marker expression tested (*RECOVERIN* t(2)=0.22,
631 p=0.85; *OTX2* t(2)=2.99, p=0.10; *RXR*γ t(3)=0.23, p=0.83; *THR*β t(2)=1.01, p=0.40; *VSX2* t(3)=0.39,
632 p=0.72). (d) Immunostaining of AGN193109 and DMSO dosed control hROs at d60 showed a significant
633 increase in proportion of cone progenitor marker OTX2+ (yellow)/DAPI+ (grey) cells in AGN193109
634 dosed hROs (t(28)=2.4, p=0.02). Further marker expression following early dosing shown in **Fig.S5**. qRT-
635 PCR data shown as Log2 fold change of CT values relative to DMSO treated controls (n=5 pooled
636 hROs/sample, N≥3). Significance values determined by paired (qPCR)/unpaired (IHC) t-tests: *p
637 value<0.05, ****p value<0.0001, n ≥13, data shown as mean±SD. Brightfield/staining images
638 representative of n≥13 hROs from N=2 batches. Scale bars: 200um.
639
640 **Fig.7. Additional late dosing of hROs with RA receptor inhibitor AGN193109 results in increased M/L-**
641 **OPSIN and reduced S-OPSIN expression, indicating shift in cone subtype specification towards fovea-**
642 **like composition.** (a) Graphs show the effects of dosing with RA receptor inhibitor AGN193109 early
643 in differentiation ("early"; d42-d50), or "early+late" (d42-50 and d70-80/d120-130) on photoreceptor
644 mRNA expression at d150. Early-only dosing had no effect on any marker expression tested: (i)
645 *ARRESTIN*-3 t(4)=1.80, p=0.15; (ii) *RHODOPSIN* t(4)=0.63, p=0.56; (iii) *S-OPSIN* (t(4)=1.06, p=0.35); (iv)

646 *M-OPSIN* $t(4)=2.3$, $p=0.08$); and (v) *L-OPSIN,* (W=9, n=5, $p=0.31$). Early+late dosing lead to (i) no change
647 in *ARRESTIN*-3, (W=-15, n=6, $p=0.16$); (ii) or *RHODOPSIN* (t(5)=2.48 $p=0.06$); (iii) a significant decrease
648 in *S-OPSIN* ($t(5)=6.68$, $p=0.001$), (iv) a significant 1.8-fold increase in *M-OPSIN* ($t(5)=2.82$, $p=0.04$) and
649 (v) a significant 3.5-fold increase in *L-OPSIN,* ($t(5)=3.27$, $p=0.02$).
650 (**b**) Addition of late pulses of AGN193109 (early+late) led to no change in proportion of DAPI+ (grey)
651 cells expressing (i) ARRESTIN-3 ($t(11)=1.29$, $p=0.22$) or (ii) RHODOPSIN ($t(11)=0.41$, $p=0.69$), (iii) but a
652 significant decrease in the proportion of ARRESTIN-3+ cells expressing (iv) S-OPSIN ($t(11)=3.14$,
653 $p=0.01$), (iv) although no change was observed in the proportion of ARRESTIN-3+ cells expressing M/L-
654 OPSIN ($t(11)=0.14$, $p=0.89$). qRT-PCR data shown as Log_2 fold change of CT values relative to DMSO
655 treated controls (n=3 pooled hROs/sample, N≥5 samples/group). Significance values determined by
656 paired (qPCR)/unpaired (IHC) t-tests or Wilcoxon test: *p value<0.05, **p value<0.01, data shown as
657 mean±SD. Staining data representative of n>5 hROs from N=2 batches. Scale bars: 500μm.

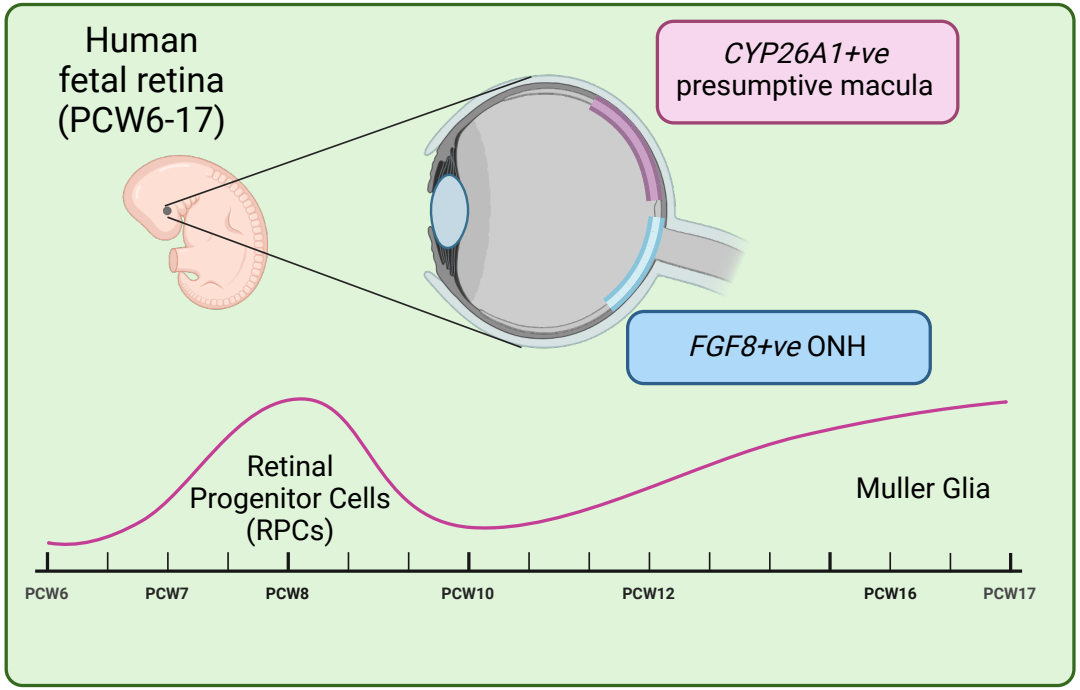
Human
fetal retina
(PCW6-17)
CYP26A1+ve
presumptive macula
FGF8+ve ONH
Retinal
Progenitor Cells
(RPCs)
Muller Glia
PCW6
PCW7
PCW8
PCW10
PCW12
PCW16
PCW17

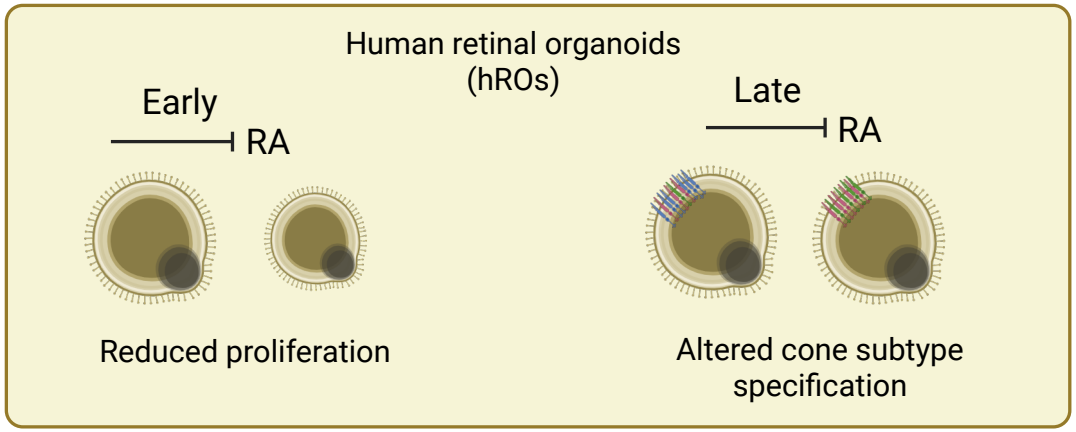
Human retinal organoids
(hROs)
Early
RA
Late
RA
Reduced proliferation
Altered cone subtype
specification

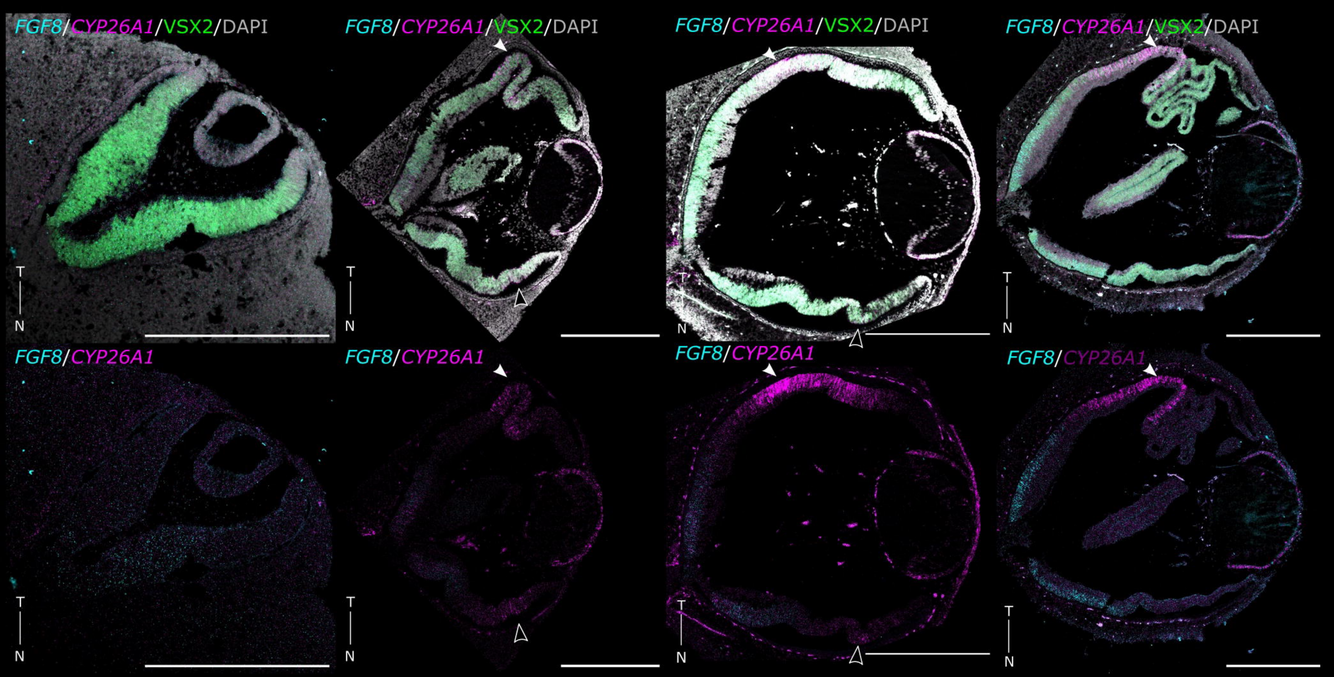
FGF8/CYP26A1/VSX2/DAPI
FGF8/CYP26A1
T
N

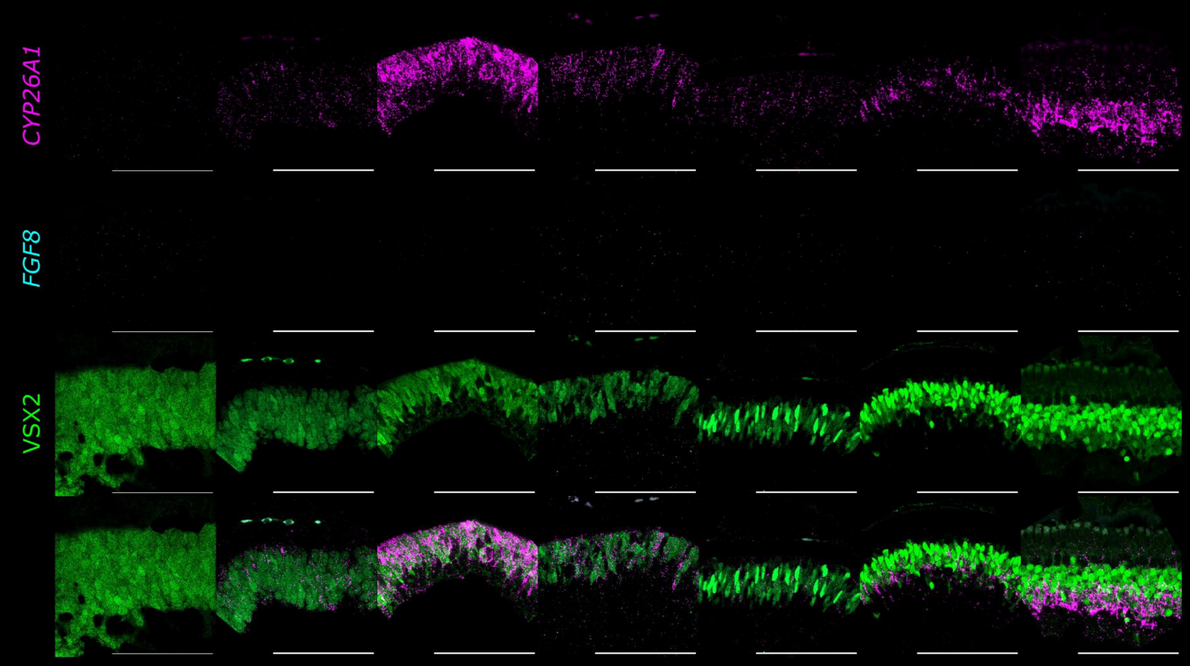
CYP26A1
FGF8
VSX2

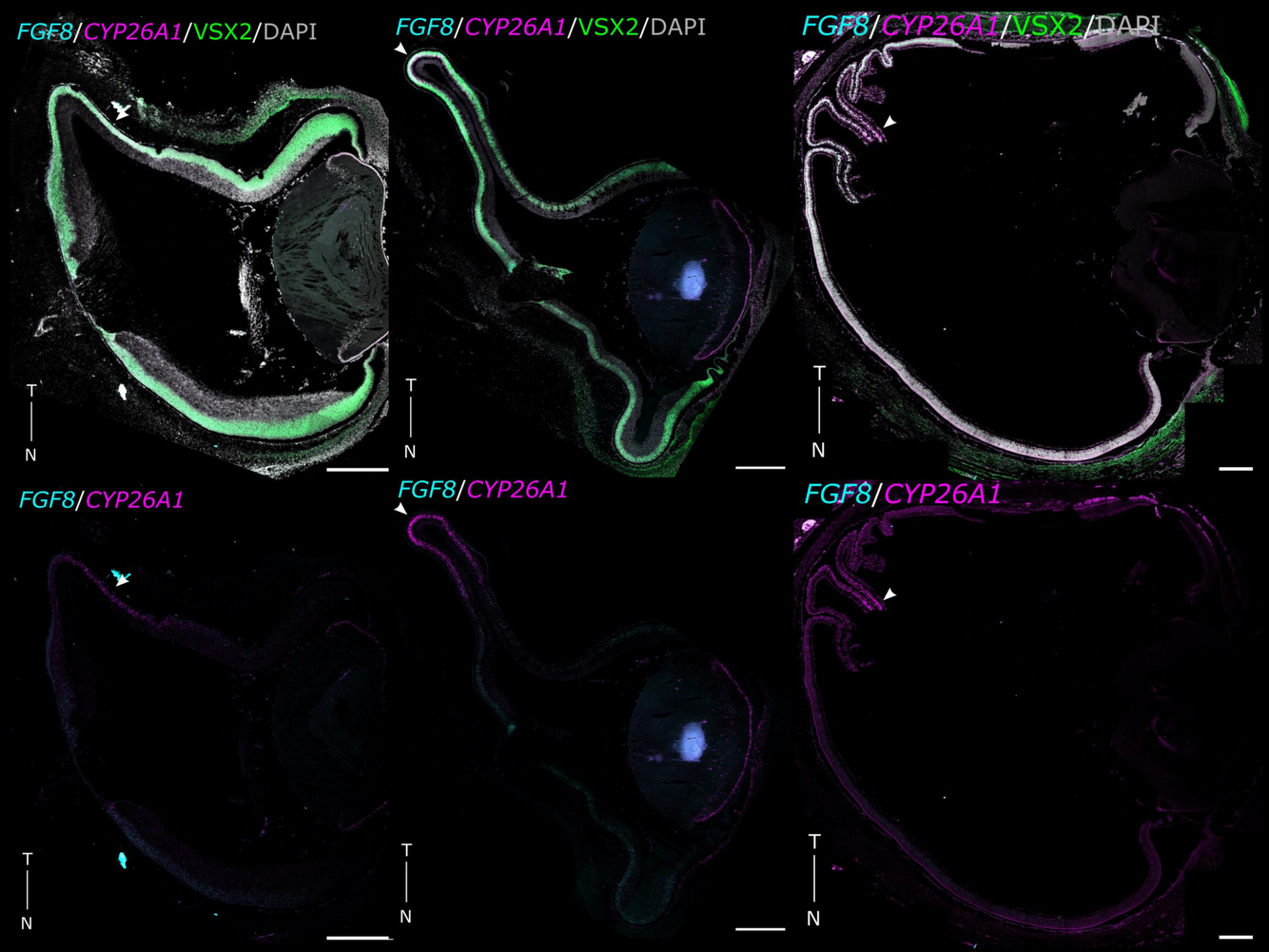
FGF8/CYP26A1/VSX2/DAPI
FGF8/CYP26A1
T
N

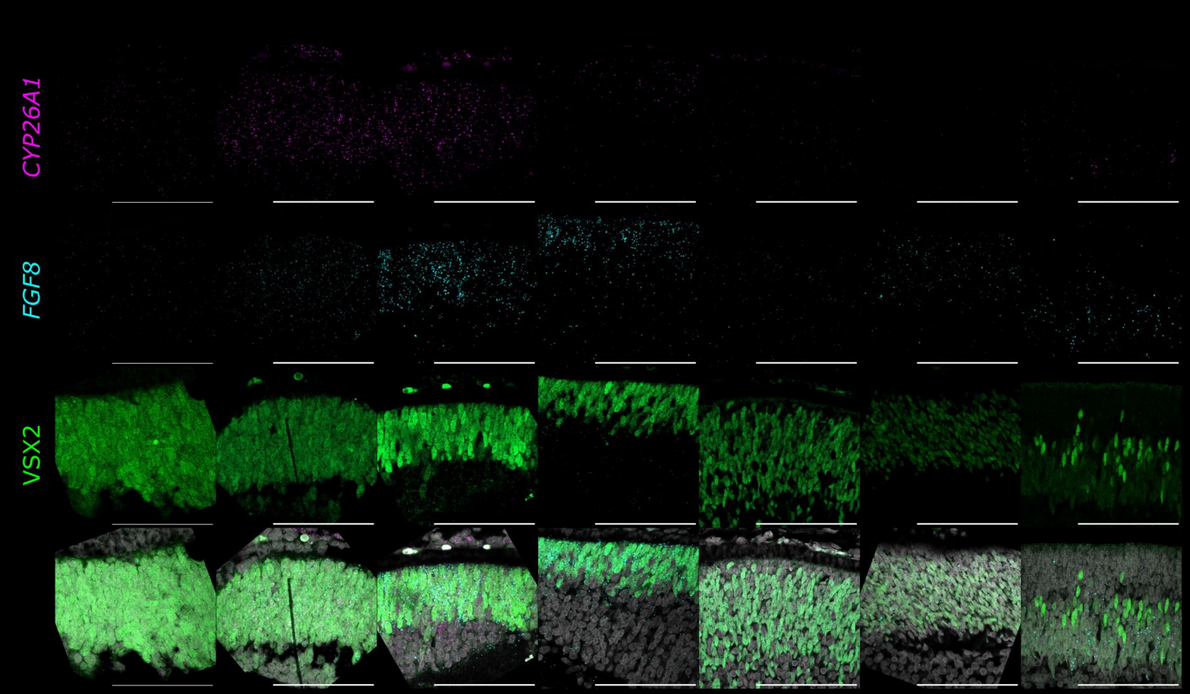
CYP26A1
FGF8
VSX2

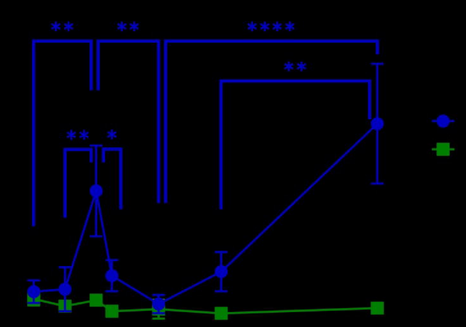
**
**
****
**
**
*

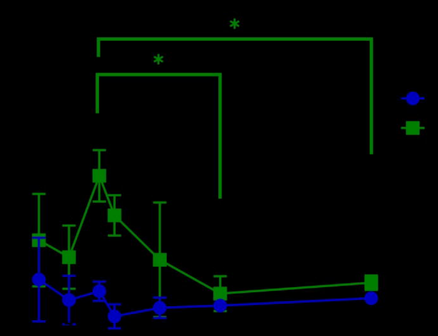
*
*

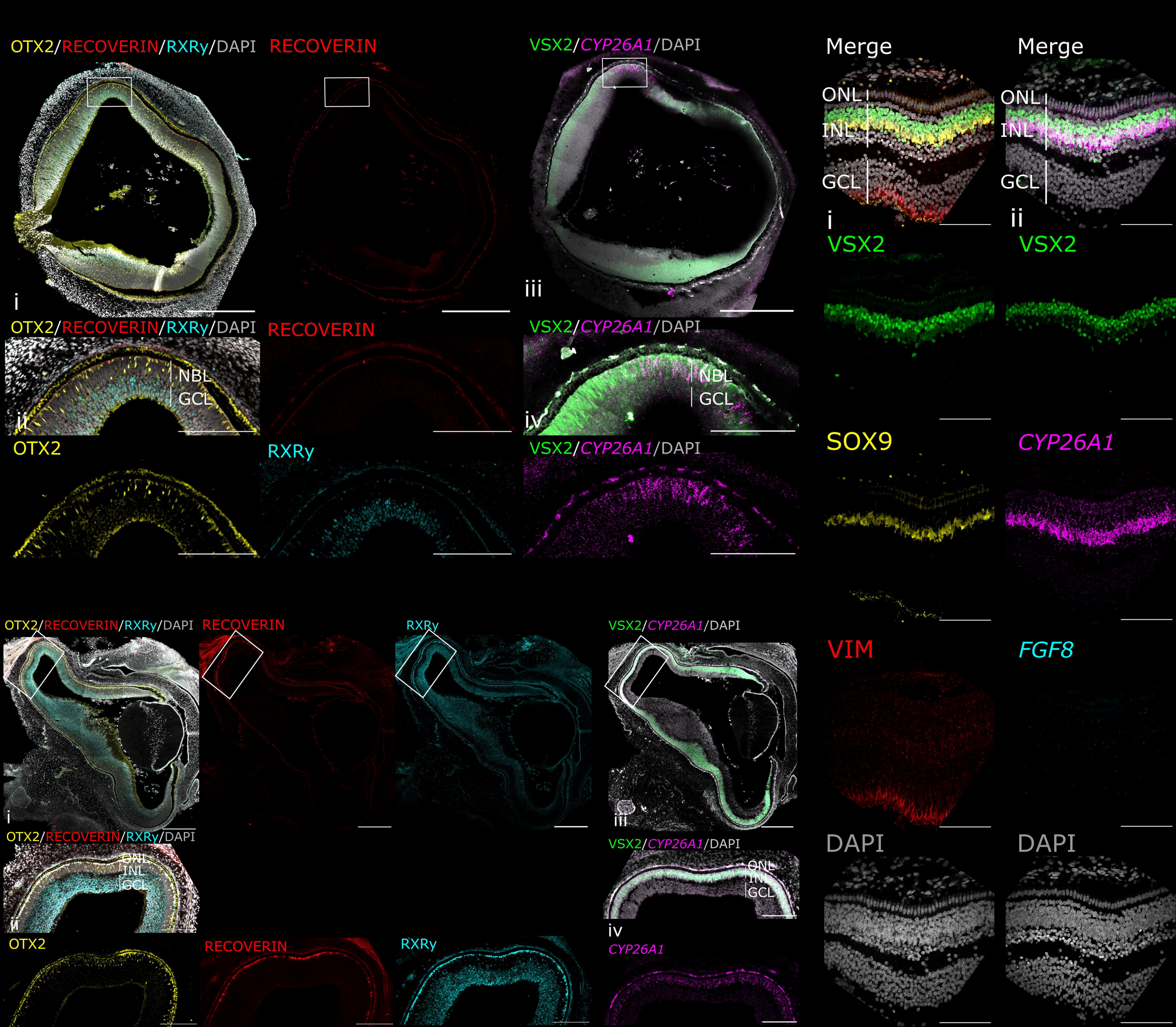
OTX2/RECOVERIN/RXRy/DAPI
RECOVERIN
VSX2/CYP26A1/DAPI
Merge
Merge
ONL
INL
GCL
ONL
INL
GCL
i
ii
iii
VSX2
VSX2
OTX2/RECOVERIN/RXRy/DAPI
RECOVERIN
VSX2/CYP26A1/DAPI
NBL
GCL
NBL
GCL
ii
iv
SOX9
CYP26A1
OTX2
RXRy
VSX2/CYP26A1/DAPI
OTX2/RECOVERIN/RXRy/DAPI
RECOVERIN
RXRy
VSX2/CYP26A1/DAPI
VIM
FGF8
i
iii
OTX2/RECOVERIN/RXRy/DAPI
VSX2/CYP26A1/DAPI
DAPI
DAPI
ONL
INL
GCL
ONL
INL
GCL
ii
iv
OTX2
RECOVERIN
RXRy
CYP26A1

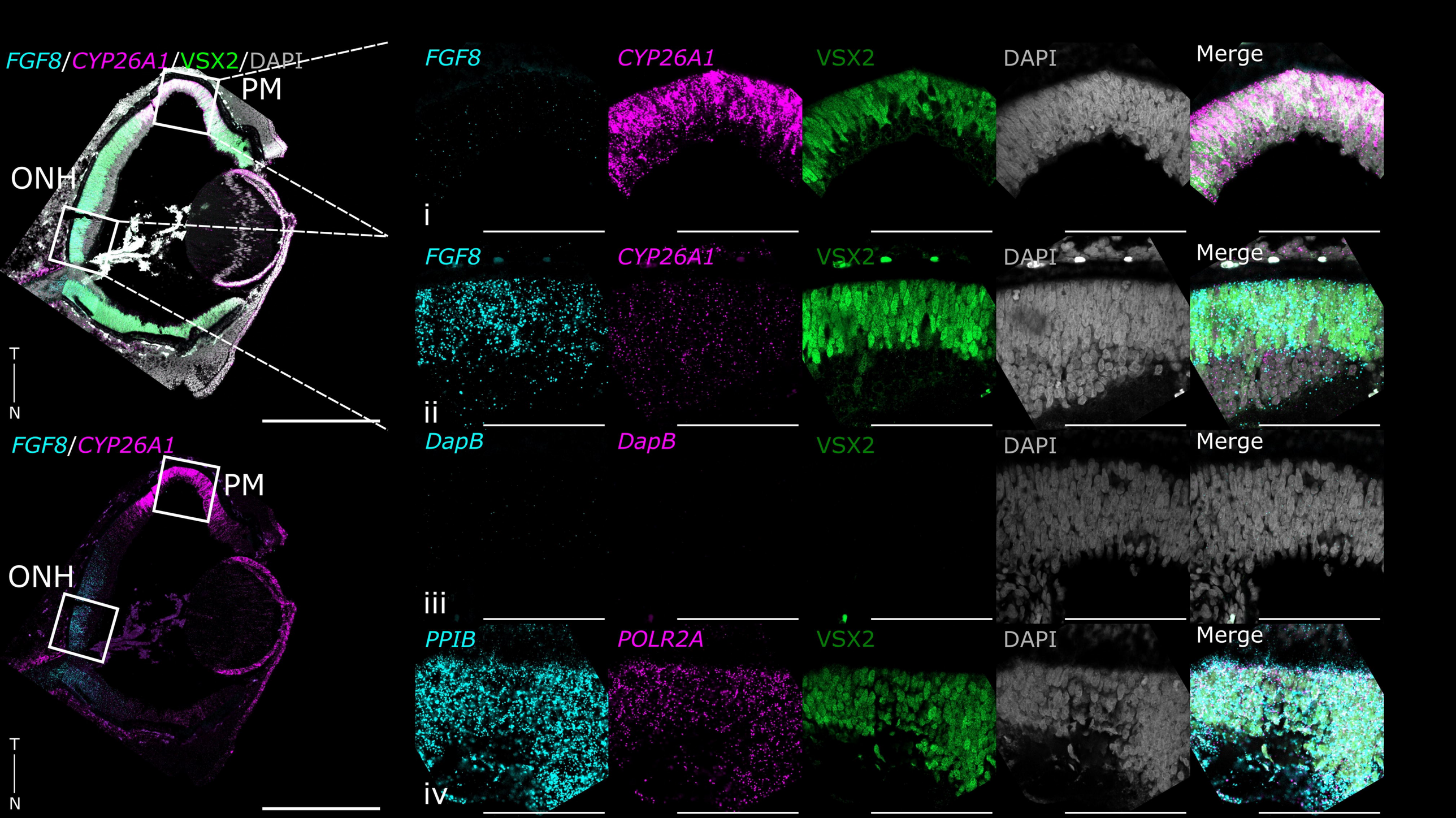
FGF8/CYP26A1/VSX2/DAPI
PM
ONH
T
N
FGF8/CYP26A1
PM
ONH
T
N
FGF8
CYP26A1
VSX2
DAPI
Merge
i
FGF8
CYP26A1
VSX2
DAPI
Merge
ii
DapB
DapB
VSX2
DAPI
Merge
iii
PPIB
POLR2A
VSX2
DAPI
Merge
iv

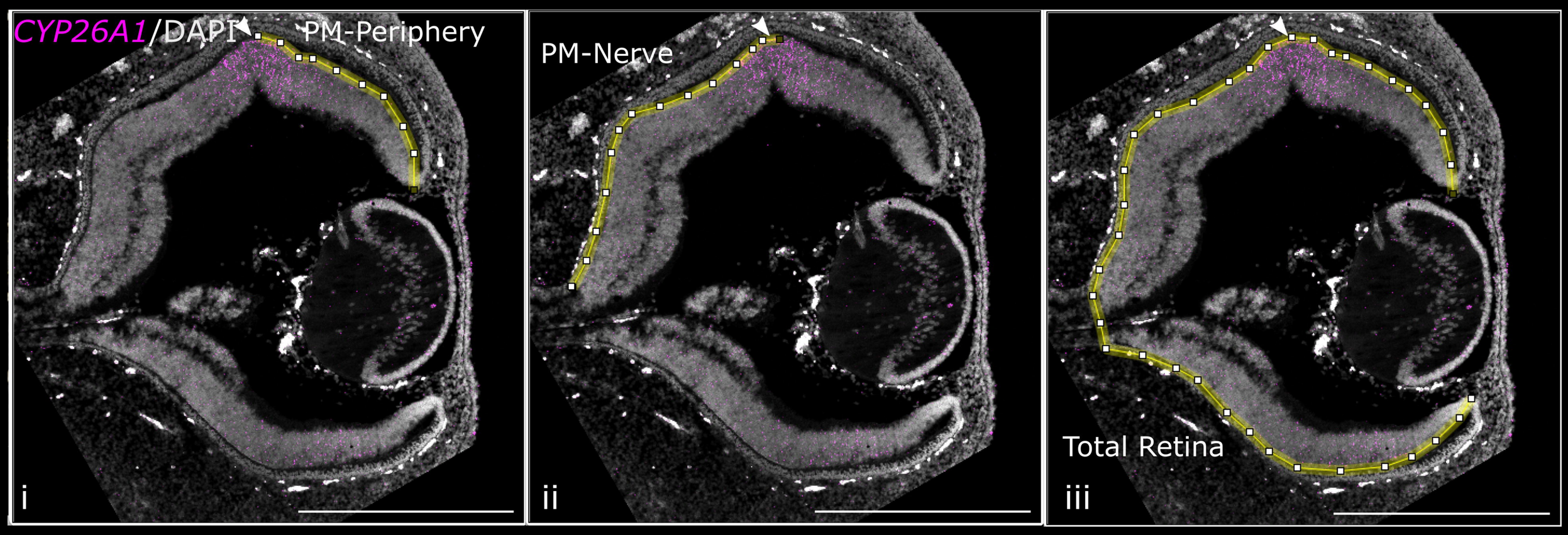
CYP26A1/DAPI
PM-Periphery
i
PM-Nerve
ii
Total Retina
iii

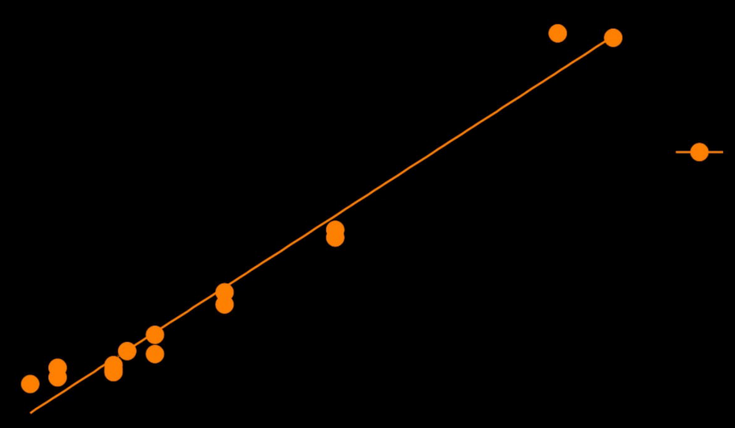

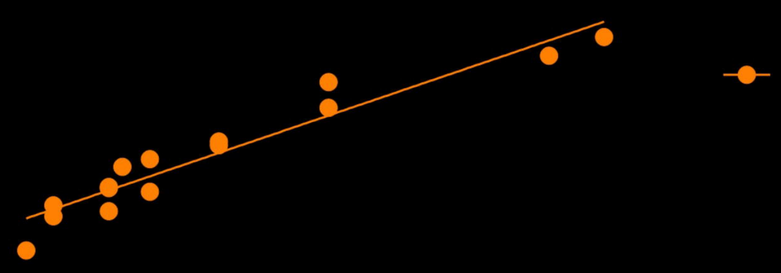

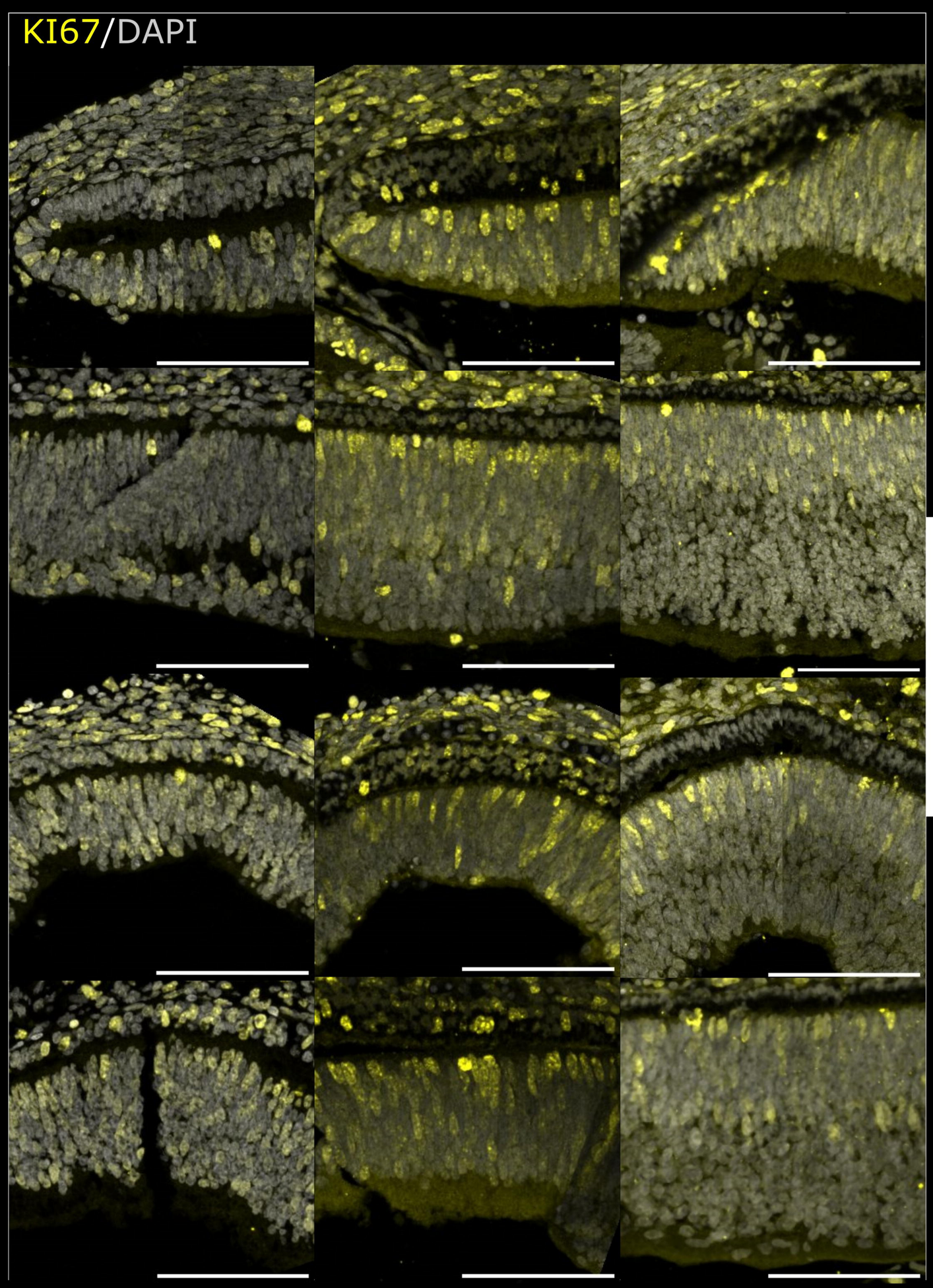
KI67/DAPI

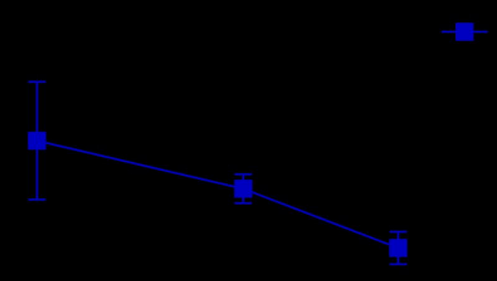

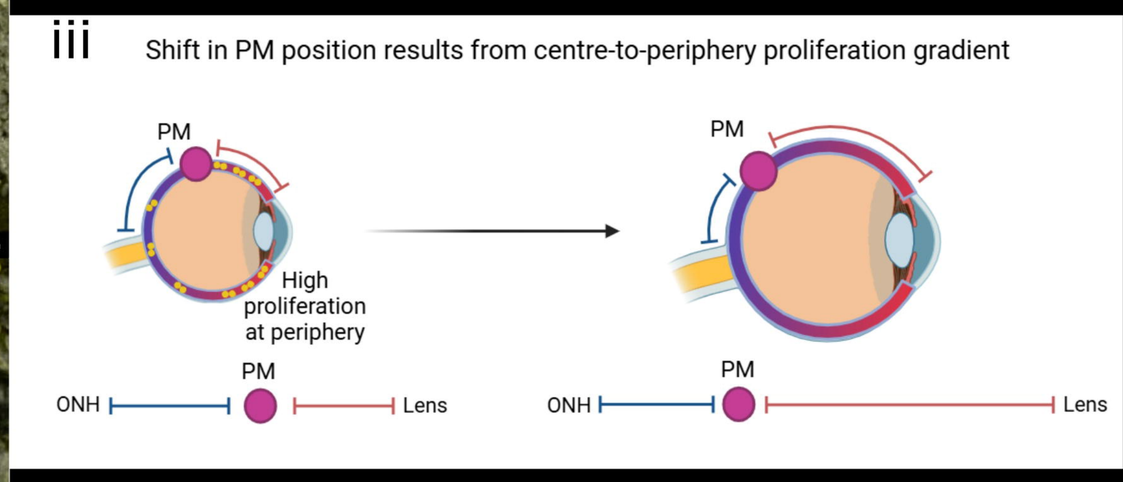
iii
Shift in PM position results from centre-to-periphery proliferation gradient
PM
High proliferation at periphery
ONH
PM
Lens
PM
ONH
PM
Lens

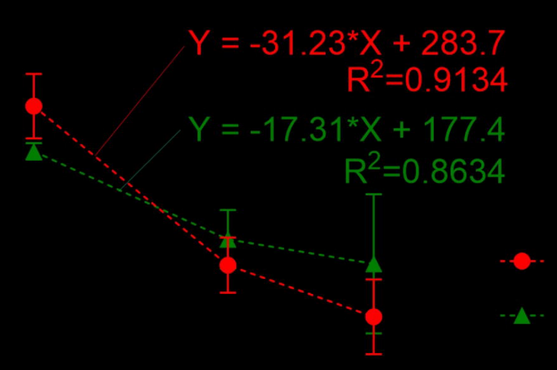
Y = -31.23*X + 283.7
R2=0.9134
Y = -17.31*X + 177.4
R2=0.8634

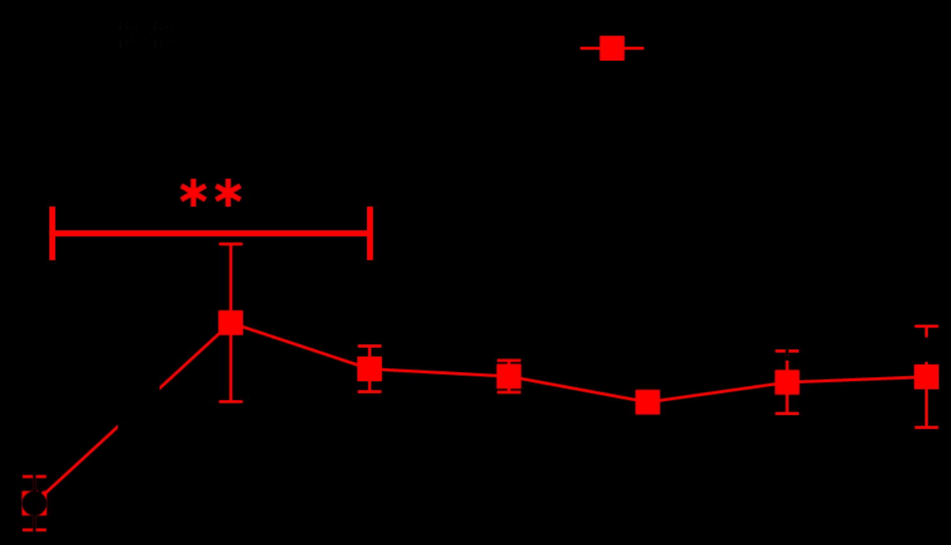
**

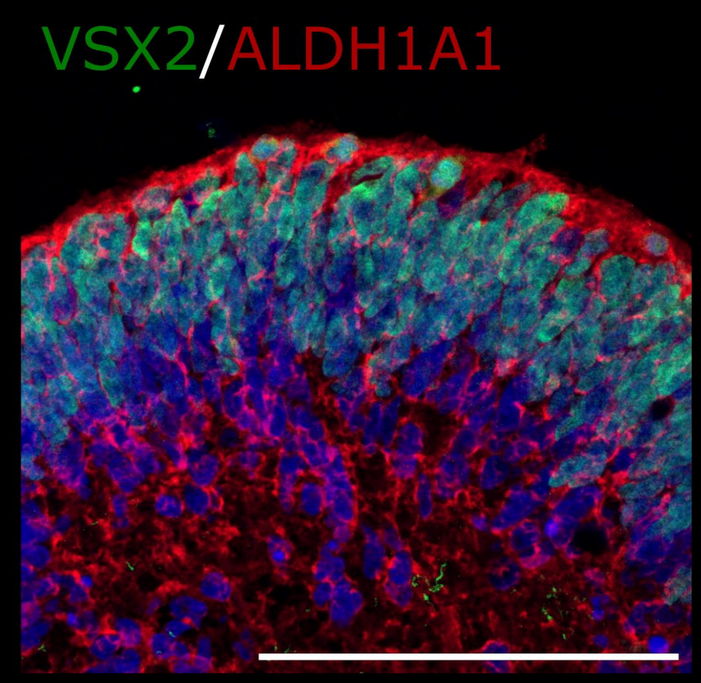
VSX2/ALDH1A1

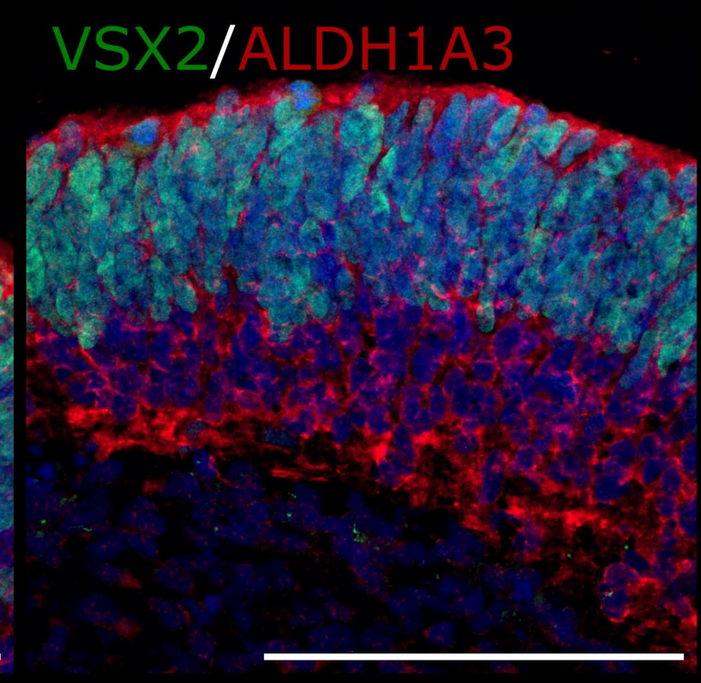
VSX2/ALDH1A3

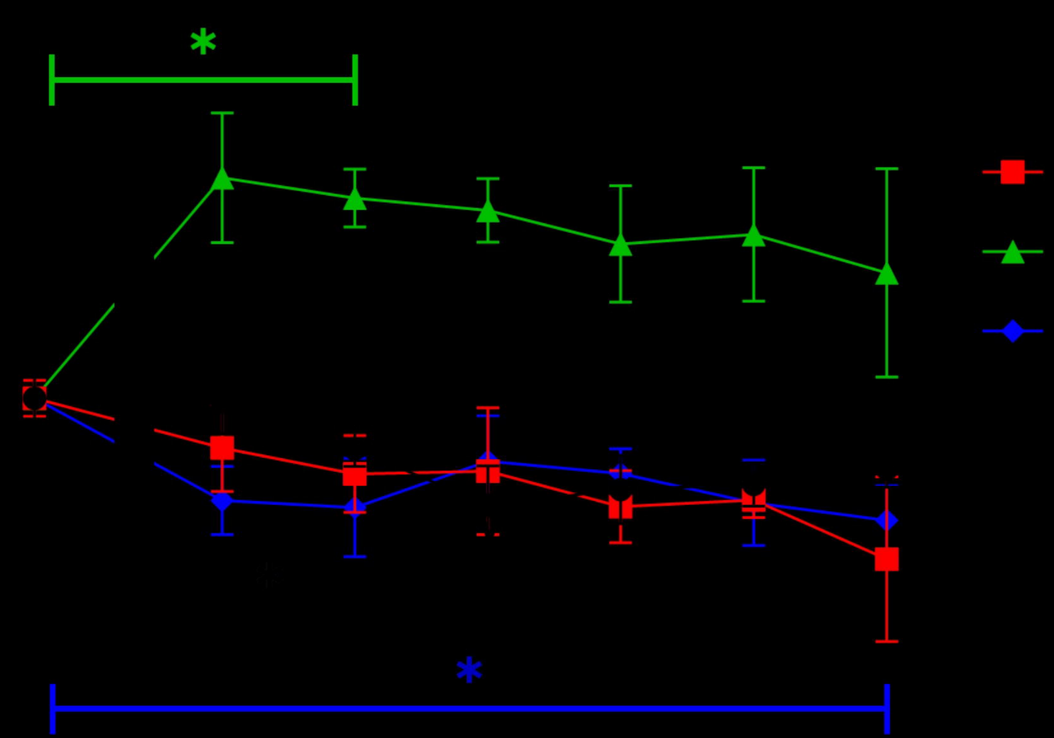
*
*

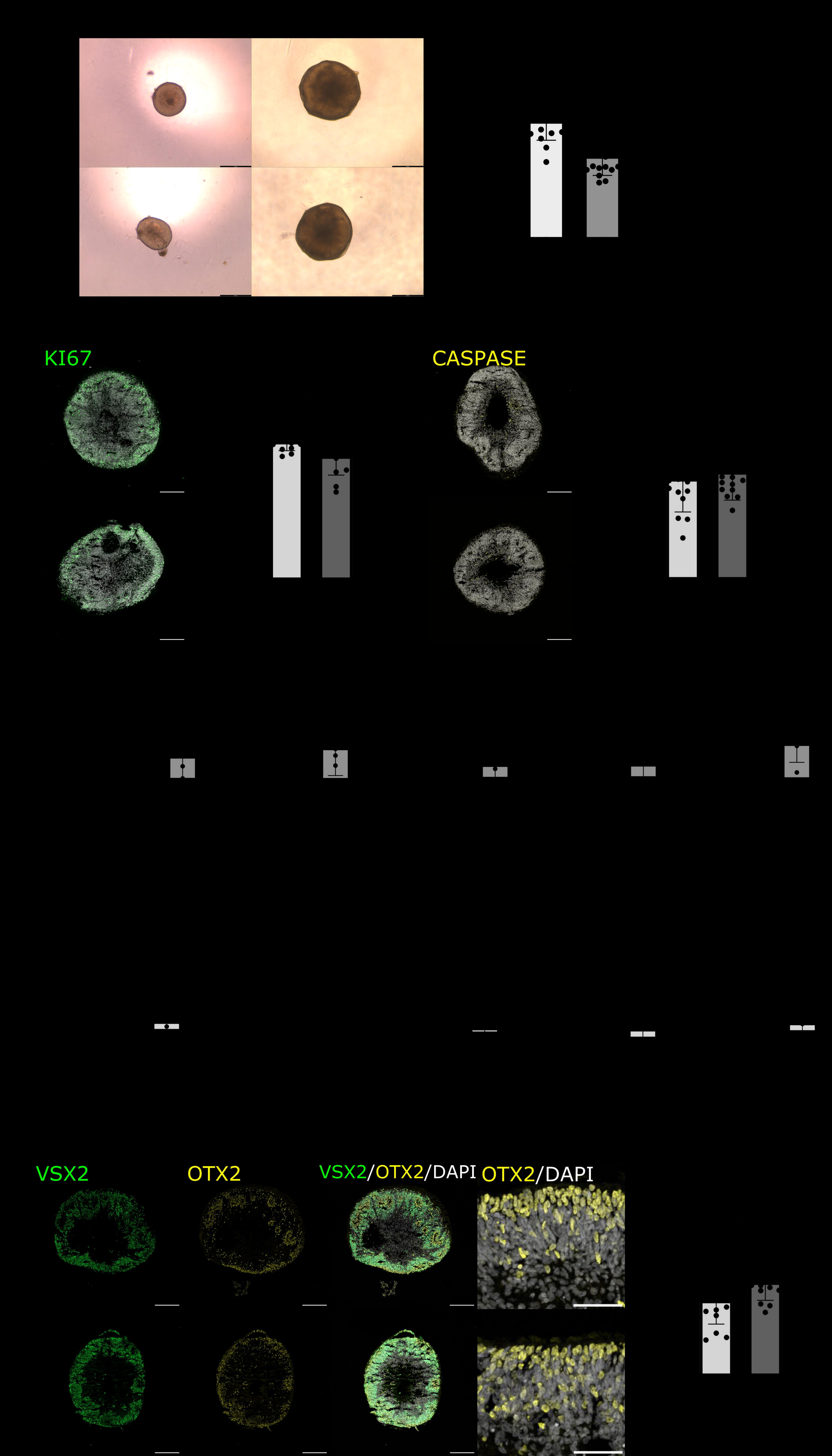
KI67
CASPASE
VSX2
OTX2
VSX2/OTX2/DAPI
OTX2/DAPI

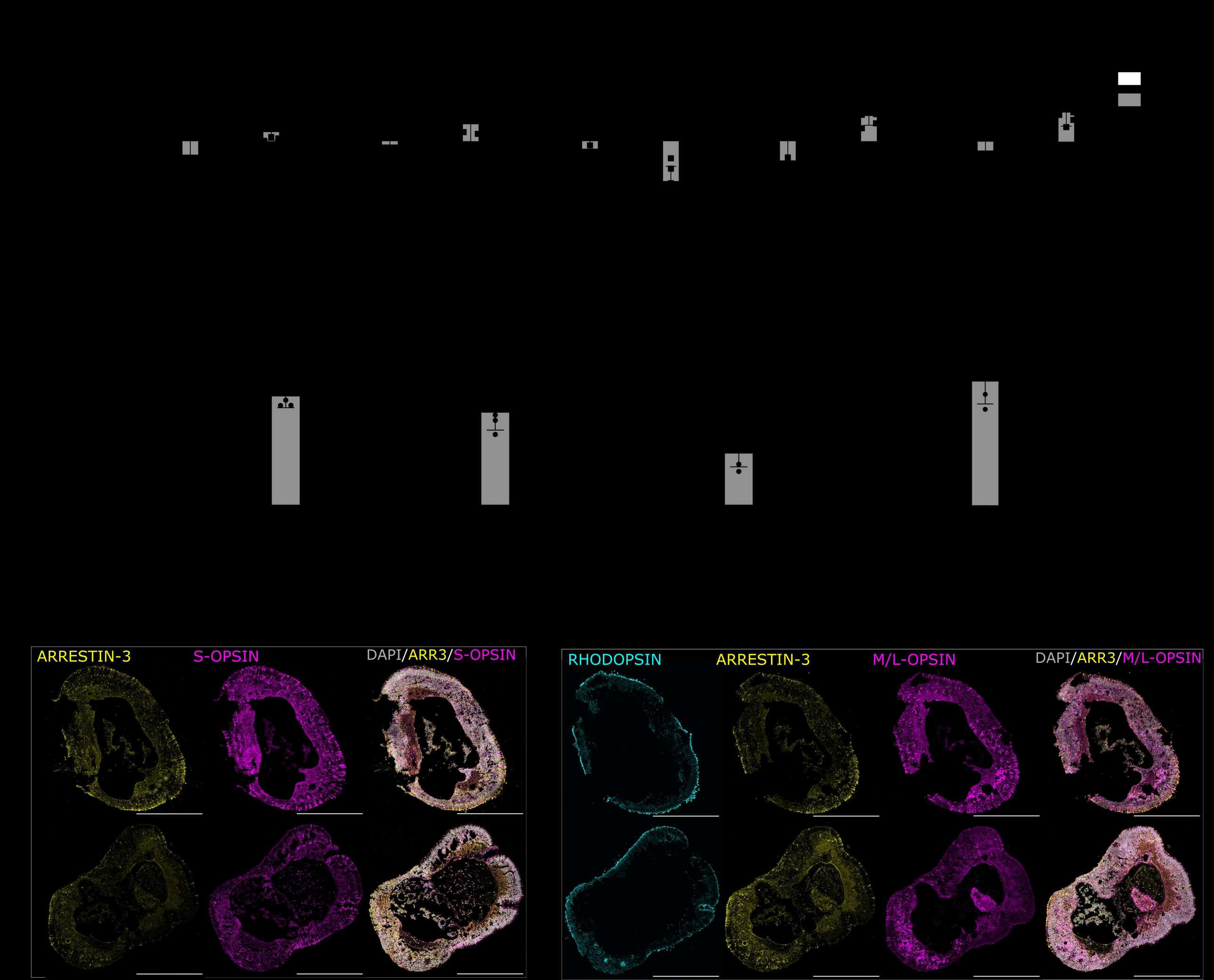
ARRESTIN-3
S-OPSIN
DAPI/ARR3/S-OPSIN
RHODOPSIN
ARRESTIN-3
M/L-OPSIN
DAPI/ARR3/M/L-OPSIN